

## RESEARCH ARTICLE

# The prion protein regulates glutamate-mediated $\text{Ca}^{2+}$ entry and mitochondrial $\text{Ca}^{2+}$ accumulation in neurons

Agnese De Mario<sup>1</sup>, Caterina Peggion<sup>1</sup>, Maria Lina Massimino<sup>2</sup>, Francesca Viviani<sup>1</sup>, Angela Castellani<sup>1</sup>, Marta Giacomello<sup>3</sup>, Dmitry Lim<sup>4</sup>, Alessandro Bertoli<sup>1,\*</sup> and Maria Catia Sorgato<sup>1,2,\*</sup>

## ABSTRACT

The cellular prion protein (PrP<sup>C</sup>) whose conformational misfolding leads to the production of deadly prions, has a still-unclear cellular function despite decades of intensive research. Following our recent finding that PrP<sup>C</sup> limits  $\text{Ca}^{2+}$  entry via store-operated  $\text{Ca}^{2+}$  channels in neurons, we investigated whether the protein could also control the activity of ionotropic glutamate receptors (iGluRs). To this end, we compared local  $\text{Ca}^{2+}$  movements in primary cerebellar granule neurons and cortical neurons transduced with genetically encoded  $\text{Ca}^{2+}$  probes and expressing, or not expressing, PrP<sup>C</sup>. Our investigation demonstrated that PrP<sup>C</sup> downregulates  $\text{Ca}^{2+}$  entry through each specific agonist-stimulated iGluR and after stimulation by glutamate. We found that, although PrP-knockout (KO) mitochondria were displaced from the plasma membrane, glutamate addition resulted in a higher mitochondrial  $\text{Ca}^{2+}$  uptake in PrP-KO neurons than in their PrP<sup>C</sup>-expressing counterpart. This was because the increased  $\text{Ca}^{2+}$  entry through iGluRs in PrP-KO neurons led to a parallel increase in  $\text{Ca}^{2+}$ -induced  $\text{Ca}^{2+}$  release via ryanodine receptor channels. These data thus suggest that PrP<sup>C</sup> takes part in the cell apparatus controlling  $\text{Ca}^{2+}$  homeostasis, and that PrP<sup>C</sup> is involved in protecting neurons from toxic  $\text{Ca}^{2+}$  overloads.

**KEY WORDS:** Neuron, Prion protein,  $\text{Ca}^{2+}$  homeostasis, Glutamate, Mitochondria,  $\text{Ca}^{2+}$ -induced  $\text{Ca}^{2+}$  release, AMPA receptor

## INTRODUCTION

A conformational remodeling of the cellular prion protein (PrP<sup>C</sup>) leads to the production of prions, the infectious particles causing fatal transmissible spongiform encephalopathies or prion diseases (Prusiner, 1998). The physiological function of PrP<sup>C</sup> – which is linked to the external side of the plasma membrane (PM) – remains, however, elusive, despite the many suggestions that PrP<sup>C</sup> is intimately involved in processes protecting against cell damage and death by triggering beneficial signals either by itself or as part of multi-protein surface receptor complexes (Roucou et al., 2004; Westergaard et al., 2007; Linden et al., 2008).

Based on the notion that  $\text{Ca}^{2+}$  signaling and PrP<sup>C</sup> share functional versatility and can both promote cell survival and death (Sorgato and Bertoli, 2009), we have investigated on the capacity of PrP<sup>C</sup> to regulate neuronal  $\text{Ca}^{2+}$  homeostasis. A close link between  $\text{Ca}^{2+}$  signaling and PrP<sup>C</sup> has already been observed in animal and cell models of prion infection, showing, for example, impairment of  $\text{Ca}^{2+}$ -dependent neuronal excitability and synaptic plasticity (reviewed in Peggion et al., 2011). The role of PrP<sup>C</sup> in  $\text{Ca}^{2+}$  homeostasis is further supported by comparing wild-type (WT) and PrP-knockout (PrP-KO) hippocampal paradigms, indicating that the absence of PrP<sup>C</sup> altered excitatory and inhibitory neurotransmission and spatial learning (Collinge et al., 1994; Mallucci et al., 2002; Criado et al., 2005; Powell et al., 2008). These studies also showed that PrP<sup>C</sup> prevented potentially toxic  $\text{Ca}^{2+}$  load mediated by the N-methyl-D-aspartate (NMDA) receptors (NMDARs), following interaction with the receptor regulatory subunit GluN2D (also known as GRIN2D) (Khosravani et al., 2008a), and by modulating the affinity for the co-agonist glycine in a copper ion-dependent manner (You et al., 2012). Seemingly, NMDARs were also implicated in the depressive-like behavior and reduced pain threshold observed in PrP-KO mice (Gadotti and Zamponi, 2011; Gadotti et al., 2012). Together with the  $\alpha$ -amino-3-hydroxy-5-methyl-4-isoxazole propionic acid (AMPA)- and kainate-responsive receptors (AMPA and kainate receptors), NMDARs belong to the glutamate-gated unselective ( $\text{Na}^+/\text{Ca}^{2+}$ ) ionotropic receptor (iGluR) channel family. iGluRs mediate the majority of rapid excitatory synaptic responses in the mammalian central nervous system (Ozawa et al., 1998), and are closely involved in models of learning and memory such as long-term potentiation (LTP) and long-term depression (LTD) (Malenka and Bear, 2004; Henley and Wilkinson, 2013). Thus, the action of PrP<sup>C</sup> on NMDARs was interpreted to prevent glutamate damage after neuronal hyper-excitation, and correlates well with the increased vulnerability observed in PrP-KO mice subjected to NMDA- (and kainate)-induced excitotoxicity (Rangel et al., 2007), as well as following epileptic seizures (Walz et al., 1999) or brain ischemia (Spudich et al., 2005).

In light of these premisses, we inspected the ability of PrP<sup>C</sup> to affect iGluR-induced  $\text{Ca}^{2+}$  movements in different domains of cerebellar granule neurons (CGNs). To this end, we used genetically targeted  $\text{Ca}^{2+}$ -sensitive probes in primary CGN cultures expressing, or not, PrP<sup>C</sup>. Our results indicated that PrP<sup>C</sup> functionally downregulates all iGluRs, and that the reduced  $\text{Ca}^{2+}$  influx attenuates the process of  $\text{Ca}^{2+}$ -induced  $\text{Ca}^{2+}$  release (CICR) under the conditions used, which in turn limits mitochondrial  $\text{Ca}^{2+}$  uptake. Some of these aspects also applied to cortical neurons. Our data thus emphasize that the beneficial action of PrP<sup>C</sup> in neurons extends beyond the PM by defending mitochondria from dangerously high  $\text{Ca}^{2+}$  accumulations.

<sup>1</sup>Department of Biomedical Science, University of Padova, 35131 Padova, Italy.

<sup>2</sup>CNR Neuroscience Institute, Department of Biomedical Science, University of Padova, 35131 Padova, Italy. <sup>3</sup>Department of Biology, University of Padova, 35131 Padova, Italy. <sup>4</sup>Department of Pharmaceutical Science, University of Piemonte Orientale, 28100 Novara, Italy.

\*Authors for correspondence (catia.sorgato@unipd.it; alessandro.bertoli@unipd.it)

© A.D.M., 0000-0003-0184-0450; C.P., 0000-0002-9967-2629; M.L.M., 0000-0002-1839-1404; F.V., 0000-0001-7391-9673; A.C., 0000-0003-2432-8126; M.G., 0000-0002-0290-6602; D.L., 0000-0002-4316-2654; A.B., 0000-0003-1202-0191; M.C.S., 0000-0001-8563-7462

## RESULTS

**PrP<sup>C</sup> attenuates iGluR-mediated Ca<sup>2+</sup> entry in CGNs and cortical neurons**

In light of the electrophysiological evidence showing that PrP<sup>C</sup> restricts NMDAR-mediated Ca<sup>2+</sup> currents in hippocampal slices and neurons (Khosravani et al., 2008a; You et al., 2012), we used Ca<sup>2+</sup>-sensitive aequorin (AEQ) probes to compare NMDA-induced Ca<sup>2+</sup> movements in specific domains of primary CGNs obtained from co-isogenic murine lines with (PrP-Tg) or without (PrP-KO) PrP<sup>C</sup>. Fig. 1 reports the kinetics of Ca<sup>2+</sup> fluxes (Fig. 1A,B, upper

panels) and the peak response (Fig. 1A,B, lower panels), detected by AEQ targeted to the inner PM subdomains (AEQ<sub>pm</sub>) (Fig. 1A) or the bulk cytosol (AEQ<sub>cyt</sub>) (Fig. 1B). Data clearly show that the absence of PrP<sup>C</sup> (black) enhanced Ca<sup>2+</sup> peaks compared to those in PrP-Tg CGNs (gray), both at the PM and in the cytosol (by more than 100% and ~25%, respectively). The sum of the Ca<sup>2+</sup> load during the first 100 s of Fig. 1A (upper panel) indicates that the Ca<sup>2+</sup> accumulation over time in PM subdomains of PrP-KO CGNs is two-fold higher (110.2±7.1 μM) than in PrP-Tg CGNs (54.3±2.5 μM) (mean±s.e.m.). Collectively, these results underline that PrP<sup>C</sup> acts as

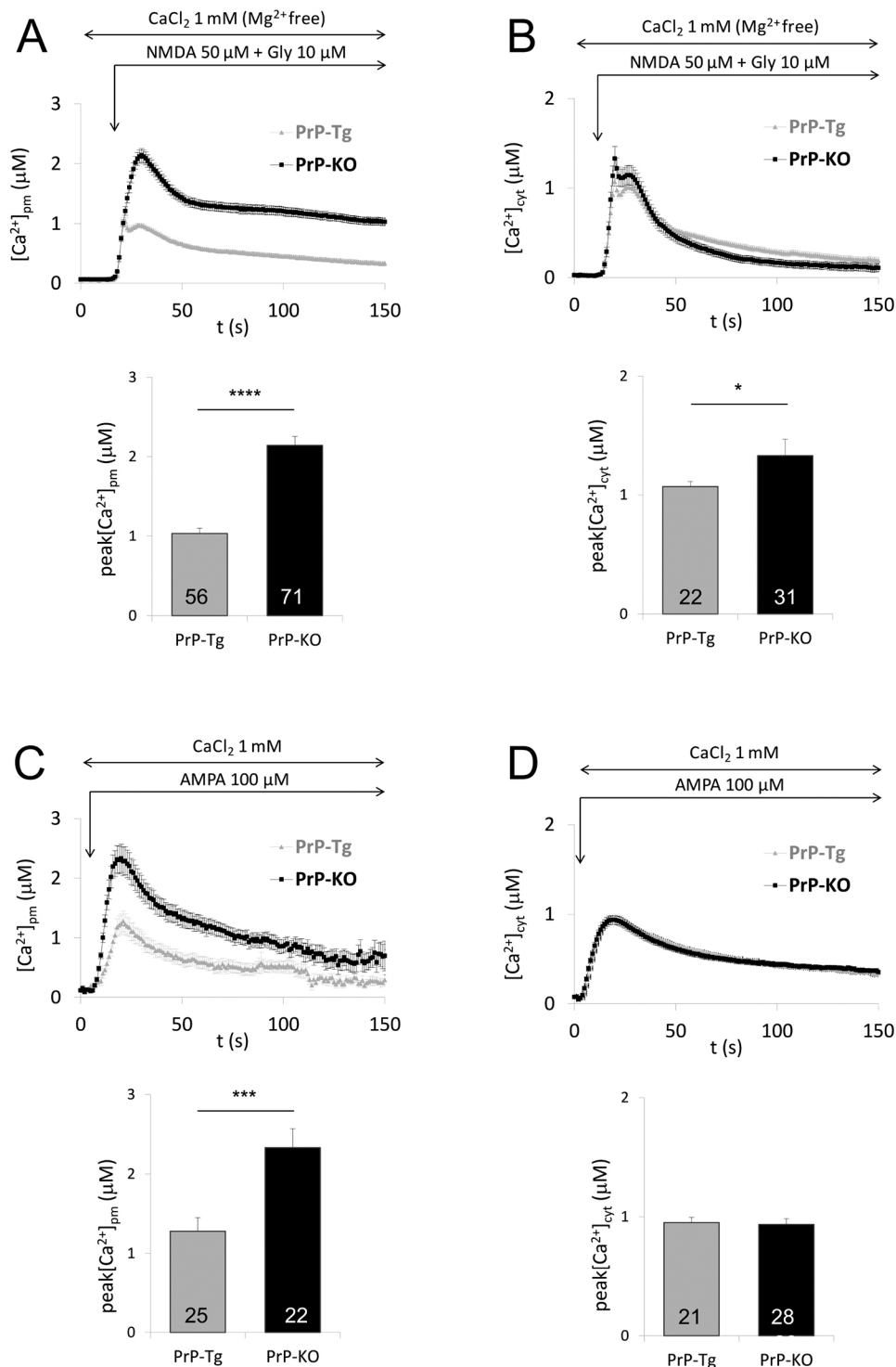


**Fig. 1. PrP<sup>C</sup> downregulates Ca<sup>2+</sup> uptake in CGNs after activation of specific iGluR types.** PrP-Tg (gray) and PrP-KO (black) CGNs were analyzed for Ca<sup>2+</sup> responses upon NMDA [in the absence of Mg<sup>2+</sup> and in the presence of NMDAR co-agonist glycine (Gly), as indicated] (A,B) or AMPA (C,D) stimulation, in plasma membrane (PM)-subdomains (A,C) or in the bulk cytosol (B,D), by use of genetically targeted AEQ<sub>pm</sub> and AEQ<sub>cyt</sub> Ca<sup>2+</sup> probes, respectively. Upper panels, showing the average kinetics of local Ca<sup>2+</sup> transients, and lower bar diagrams, reporting the corresponding Ca<sup>2+</sup> peaks, indicate that NMDA and AMPA induced significantly higher PM Ca<sup>2+</sup> transients in PrP-KO than in the PrP-Tg counterpart, by more than 100% and ~80%, respectively. The higher percentage difference observed in PM subdomains after activation of NMDARs than AMPARs might explain why a slight, though significant, percentage difference (by ~25%) could be detected in cytosolic Ca<sup>2+</sup> levels between PrP-KO and PrP-Tg CGNs only following NMDA addition (for more details, see the text). Values are expressed as mean±s.e.m., and the number of replicates (i.e. different coverslips from at least three primary CGN cultures prepared on different days) is indicated inside each diagram bar. \**P*<0.05, \*\*\**P*<0.001, \*\*\*\**P*<10<sup>-5</sup> (Student's *t*-test).

a modulator of NMDARs also in CGNs. Notably, activity of NMDARs generated similar long-lasting and higher PM  $\text{Ca}^{2+}$  amount in primary PrP-KO cortical neurons than in PrP-Tg counterparts (Fig. S1A).

Next, we investigated whether PrP<sup>C</sup> could control AMPA-sensitive iGluRs. As shown (Fig. 1C), addition of AMPA generated PM  $\text{Ca}^{2+}$  peaks that in PrP-KO neurons were ~80% enhanced compared to those in PrP-Tg CGNs. However, no significant difference in cytosolic  $\text{Ca}^{2+}$  peaks was detected (Fig. 1D), in contrast to what observed upon NMDA stimulation. In this respect, it is to be noted that what is sensed by AEQpm in PM  $\text{Ca}^{2+}$  hot spots (Filadi and Pozzan, 2015) would not be expected to correspond to the  $\text{Ca}^{2+}$  levels detected by AEQcyt. Indeed, not only does AEQcyt monitor the average bulk cytosolic  $\text{Ca}^{2+}$ , but also diverse cytosolic  $\text{Ca}^{2+}$  levels may arise only when the corresponding  $\text{Ca}^{2+}$  difference in PM subdomains is above a given threshold. This contention is further corroborated by the calculated sum of the  $\text{Ca}^{2+}$  load over the time-to-peak period in PrP-KO CGNs compared to the PrP-Tg counterpart, which resulted in three-fold greater  $\text{Ca}^{2+}$  amounts following stimulation by NMDA ( $29.7 \pm 1.1 \mu\text{M}$  in PrP-KO CGNs;  $9.9 \pm 1.3 \mu\text{M}$  in PrP-Tg CGNs;  $P < 0.001$ ), and less than two-fold greater after AMPA ( $23.7 \pm 2.1 \mu\text{M}$  in PrP-KO CGNs;  $13.1 \pm 1.5 \mu\text{M}$  in PrP-Tg CGNs;  $P < 0.001$ ) addition. PM  $\text{Ca}^{2+}$  transients of much smaller amplitude were observed upon kainate addition, and yet again they were significantly lower in PrP-Tg than in PrP-KO CGNs (data not shown).

#### Possible mechanisms for PrP<sup>C</sup> regulation of NMDARs and AMPARs in CGNs

A major way to regulate the function of NMDARs and AMPARs is via the reversible phosphorylation of their subunits (Lussier et al.,

2015). NMDARs, for example, are obligatory heterotetramers, comprising two GluN1 (also known as GRIN1) subunits and two GluN2A-D/GluN3A-B subunits (Paoletti et al., 2013). Of those, GluN2A and GluN2B harbor Tyr residues at seven different positions that can be phosphorylated by the Src family kinase (SFK) member Fyn. Of these, phosphorylation of Tyr1472 (positioned in GluN2B subunits) is necessary for preventing endocytosis of NMDARs and for stabilizing the receptor in synaptic membranes (Nakazawa et al., 2001; Trepanier et al., 2012). Thus, because we have shown that PrP<sup>C</sup> constitutively downregulates Fyn in CGNs (De Mario et al., 2015), NMDAR-induced PM  $\text{Ca}^{2+}$  fluxes were analyzed in the presence of the SFK inhibitor saracatinib, or the less-specific kinase inhibitor PP2, to understand whether the PrP<sup>C</sup>–Fyn link controlled NMDARs. Fig. 2 reports that saracatinib (Fig. 2B) and, to a greater extent, PP2 (Fig. 2C) reduced PM  $\text{Ca}^{2+}$  peaks in both CGN genotypes. Both inhibitors, however, were unable to abrogate the  $\text{Ca}^{2+}$  peak difference observed in their absence (Fig. 2A). This result indicates that SFK and non-SFK members may stabilize NMDARs on the CGN PM and/or regulate the receptor function (Lussier et al., 2015), but that their activity cannot account for the difference in NMDAR-mediated  $\text{Ca}^{2+}$  fluxes observed in the two genotypes. Next, in light of the recently proposed axis between PrP<sup>C</sup> and  $\text{Ca}^{2+}$ /calmodulin-dependent protein kinase II (CaMKII) (Haas et al., 2016), and the notion that CaMKII controls NMDAR recycling by phosphorylating GluN2B subunits (on Ser1303) (Lussier et al., 2015), we examined whether a different basal active state of CaMKII (on the Thr286 autophosphorylation site) could account for the dissimilar  $\text{Ca}^{2+}$  entry observed in the two CGN genotypes. This analysis, however, showed comparable results in PrP-Tg and PrP-KO CGNs (Fig. S2A). Taken together, obtained results suggest that other (Fyn- and CaMKII-independent)

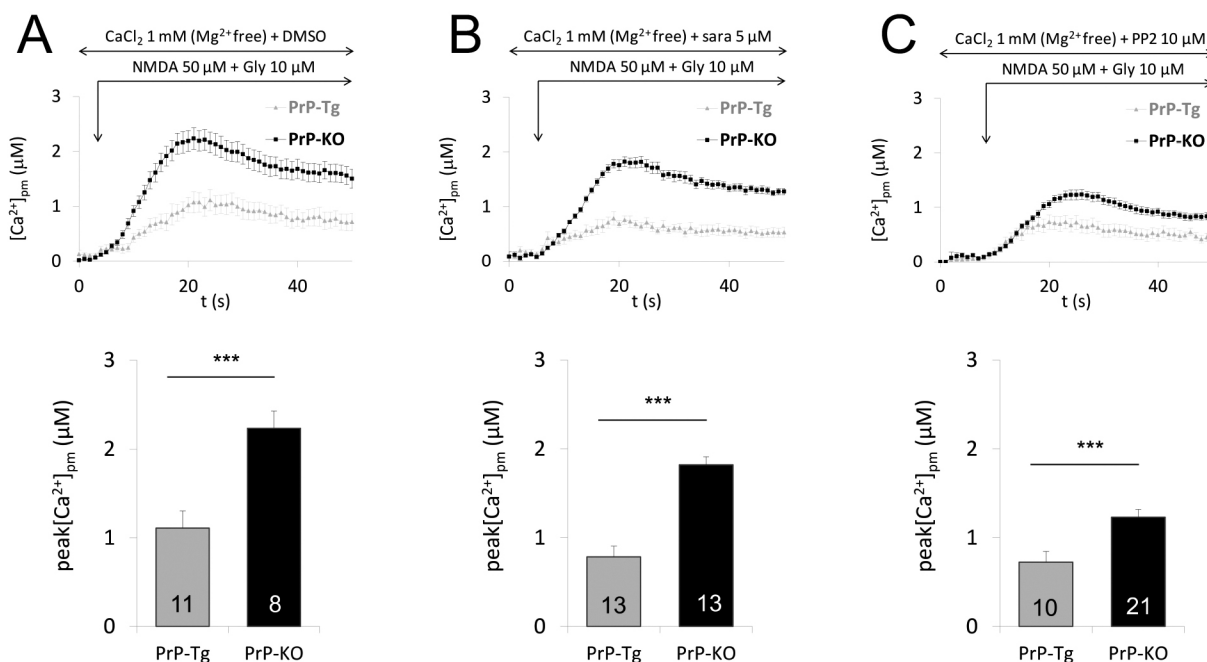


**Fig. 2. The difference in the NMDA-induced PM  $\text{Ca}^{2+}$  peak between PrP-Tg and PrP-KO CGNs does not depend on the activity of SFK members.** PrP-Tg (gray) and PrP-KO (black) CGNs were analyzed for  $\text{Ca}^{2+}$  fluxes in PM subdomains, by use of the AEQpm probe, after NMDA stimulation in the presence of the SFK-inhibitor saracatinib (sara) (B), the less-specific kinase inhibitor PP2 (C) or the vehicle DMSO (0.01% v/v) (A). Upper panels report the average kinetics of AEQpm-detected  $\text{Ca}^{2+}$  transients in PM-subdomains, while lower bar diagrams report the corresponding  $\text{Ca}^{2+}$  peaks, showing that both saracatinib and (to a larger extent) PP2, decrease NMDA-induced PM  $\text{Ca}^{2+}$  peaks in both PrP-Tg and PrP-KO CGNs, without, however, abrogating the difference observed in DMSO-treated CGNs. Values are expressed as mean  $\pm$  s.e.m., and the number of replicates (i.e. different coverslips from at least three primary CGN cultures prepared on different days) is indicated inside each diagram bar. \*\*\* $P < 0.001$  (Student's *t*-test).



mechanisms could play a prominent role in the regulation of the receptor metabolism and/or activity by PrP<sup>C</sup>.

Phosphorylation events on tetrameric AMPAR-forming GluR1–GluR4 (also known as GRIA1–GRIA4) subunits play a key role in modulating the receptor properties and trafficking (Lee et al., 2010; Huganir and Nicoll, 2013; Diering et al., 2016). In particular, CaMKII and cAMP-dependent protein kinase (PKA) affect the conductance (Barria et al., 1997; Kristensen et al., 2011) and opening probability (Blackstone et al., 1994; Banke et al., 2000) of AMPAR channels by acting on Ser831 and Ser845 of the GluR1 subunit, respectively. PKA-mediated Ser845 phosphorylation, however, also promotes GluR1 insertion into the PM (Diering et al., 2016). On this basis, after assessing that PrP-Tg and PrP-KO CGNs contained equal amounts of GluR1 (data not shown), we investigated on the phosphorylation state of Ser831 and Ser845 under basal conditions. Of them, Ser831, as expected, had equal (CaMKII-dependent) phosphorylation levels in the two neuronal types (Fig. S2B), whereas Ser845 was more highly phosphorylated in PrP-KO CGNs (Fig. S2C). According to Song et al. (2013), a way to enhance PKA activity is via extracellular signal-regulated kinase 1 and 2 (ERK1/2; also known as MAPK3 and MAPK1, respectively), which phosphorylate and inhibit the cAMP-hydrolyzing enzyme phosphodiesterase (PDE). Interestingly, we found that PrP-KO CGNs had ~50% more active ERK1/2 than PrP-Tg counterparts under basal conditions (Fig. S2D). This result implies that, in accordance with previous studies comparing WT and PrP-KO organotypic retinal explants (Chiarini et al., 2002), PrP-KO CGNs harbor higher cAMP, and consequently higher active PKA, levels.

To experimentally verify the consequences of the latter result, we monitored GluR1 expression at the PM through a surface biotinylation assay under basal conditions. This approach showed that the surface expression of GluR1 was ~70% more abundant in PrP-KO neurons than in PrP-Tg CGNs (Fig. 3), indicating that an enriched presence of the receptor at the PM could have contributed to the higher AMPAR-mediated Ca<sup>2+</sup> entry observed in PrP-KO CGNs.

### The complex regulation by PrP<sup>C</sup> of mitochondrial Ca<sup>2+</sup> uptake in CGNs

Finely tuned mitochondrial Ca<sup>2+</sup> transients serve to stimulate pyruvate dehydrogenase and other enzymes of the tricarboxylic acid cycle, which provide reducing equivalents necessary for ATP production by the oxidative phosphorylation process (Glancy and Balaban, 2012). Excessive mitochondrial Ca<sup>2+</sup> may, however, threaten the life of the cell through a Ca<sup>2+</sup>-dependent permeability change of the inner mitochondrial membrane, which collapses the membrane potential and releases ATP and other key molecules from the matrix, and pro-apoptotic factors from the intermembrane space (Bernardi et al., 2015).

### PrP<sup>C</sup> limits mitochondrial Ca<sup>2+</sup> uptake after glutamate addition

In light of the above notions, we used an AEQ probe targeting the mitochondrial matrix (AEQmit) to analyze the influence of PrP<sup>C</sup> over mitochondrial Ca<sup>2+</sup> uptake. Surprisingly, in spite of the smaller PM Ca<sup>2+</sup> entry observed in PrP<sup>C</sup>-expressing CGNs after addition of each iGluR agonist (NMDA or AMPA), the same protocols generated a higher (~10% with NMDA, and ~70% with AMPA) mitochondrial Ca<sup>2+</sup> peak in PrP-Tg CGNs than in PrP-KO neurons (Fig. 4).

It is important to note that ablation of the PrP-encoding gene did not alter aspects of mitochondria directly implicated in Ca<sup>2+</sup> accumulation (Fig. S3), for example, the magnitude of the mitochondrial membrane potential ( $\Delta\psi_m$ ) (Fig. S3A), and the expression level of

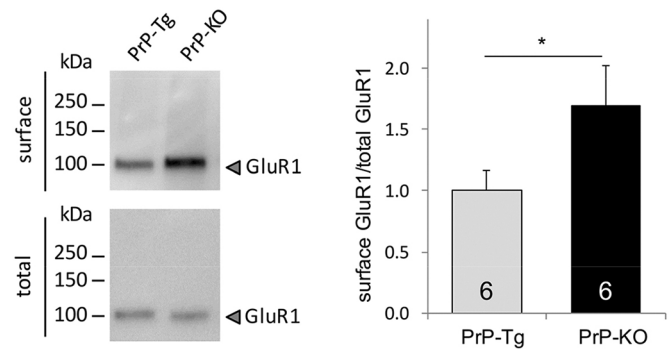


**Fig. 3. PrP<sup>C</sup> downregulates the plasma membrane localization of the GluR1 subunit of AMPARs.** Cell surface proteins were biotinylated in intact PrP-Tg and PrP-KO CGNs, and precipitated from cell lysates (300 µg of total proteins) using streptavidin-coated magnetic beads (see details in Materials and Methods). After elution, biotinylated proteins ('surface' proteins, left-upper panel), and proteins (10 µg) from cell lysates not subjected to the precipitation step ('total' proteins, left-lower panel), were analyzed by western blotting with the anti-GluR1 Ab. Western blots on the left are representative of six independent experiments (i.e. using cultures prepared in different days), while the bar diagram (right panel) reports the densitometric analysis of biotinylated GluR1 bands normalized to the corresponding total GluR1 immunosignal (after a first normalization of each immunosignal to the optical density of the respective Coomassie-stained lane; see Material and Methods). By diminishing the (PKA-dependent) phosphorylation of the AMPAR subunit GluR1 at Ser845 (see Fig. S2C), PrP<sup>C</sup> also diminishes the here-shown presence of (GluR1-containing) receptors at the cell surface that likely contribute to the smaller AMPAR-mediated Ca<sup>2+</sup> influx observed in PrP-Tg CGNs compared to PrP-KO counterparts (see Fig. 1C). Data were normalized to the values obtained with PrP-Tg samples and are expressed as mean ± s.e.m. \**P* < 0.05 (Student's *t*-test).

the channel-forming subunit of the mitochondrial Ca<sup>2+</sup> uniporter (MCU) (Fig. S3B), both of which were independent of the CGN genotype. Equally independent was the total mitochondrial density estimated according to: (1) a western blotting-mediated quantification of mitochondrial succinate dehydrogenase subunit A (SDHA) (Fig. S3C); (2) transmission electron microscopy (TEM) assessing the number of mitochondria (Fig. S3D); and (3) immunocytochemistry tracking the outer membrane component TOM20 (also known as TOMM20) (data not shown).

However, a closer analysis of ultra-thin CGN sections unexpectedly revealed that the average distance of mitochondria from the PM was ~40% larger in PrP-KO than in PrP-Tg neurons (Fig. 5). Mitochondria accumulate Ca<sup>2+</sup> from different sources depending on the cell type (Filadi and Pozzan, 2015). A major source of mitochondrial Ca<sup>2+</sup> in neurons is the extracellular space (Murgia and Rizzuto, 2015) through the activity of PM Ca<sup>2+</sup> channels (here iGluR channels). Data in Figs 4 and 5 thus support the possibility that, despite each iGluR delivering a smaller PM Ca<sup>2+</sup> quantity in PrP-Tg than in PrP-KO CGNs (Fig. 1A,C), Ca<sup>2+</sup> uptake by mitochondria of PrP-Tg CGNs was favored because of their closer proximity to the PM.

We then examined neurons exposed to glutamate, the physiological agonist for all GluRs (i.e. both ionotropic and metabotropic receptors). As predicted from the simultaneous activation of all iGluRs, use of AEQpm showed that glutamate addition elicited higher peak Ca<sup>2+</sup> transients than with each agonist (NMDA or AMPA) alone in CGNs of either genotype (Fig. 6A; compare with Fig. 1A,C). Furthermore, and different from what is observed upon stimulation by NMDA or AMPA, exposure to glutamate also led to a higher (by ~40%) Ca<sup>2+</sup> uptake in mitochondria of PrP-KO neurons compared to PrP-Tg

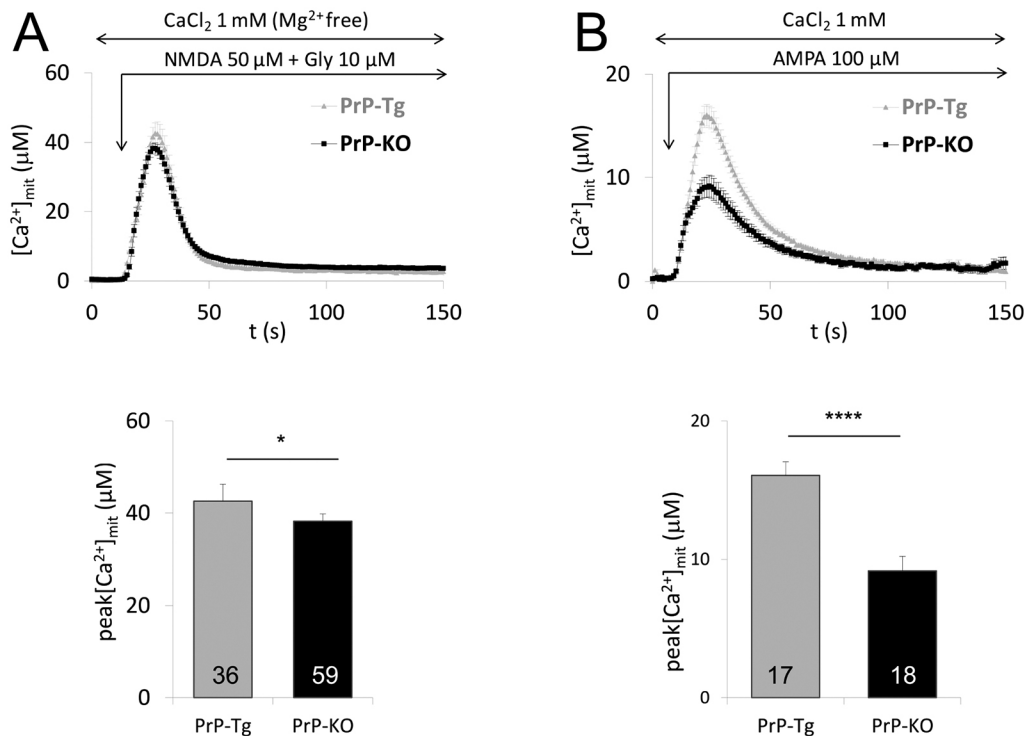


**Fig. 4. Mitochondria of PrP-KO CGNs accumulate less  $Ca^{2+}$  than PrP-Tg CGNs after activation of NMDARs or AMPARs.** CGNs were analyzed for mitochondrial  $Ca^{2+}$  responses upon NMDA (A) or AMPA (B) stimulation, by means of the AEQmit probe targeting the mitochondrial matrix. Upper and lower panels, reporting the average kinetics of  $Ca^{2+}$  transients and the corresponding  $Ca^{2+}$  peak values, respectively, indicate that, following both stimuli, PrP-Tg mitochondria accumulate more  $Ca^{2+}$  than the PrP-KO counterpart. Values are expressed as mean  $\pm$  s.e.m., and the number of replicates (i.e. different coverslips from at least three primary CGNs cultures prepared on different days) is indicated inside each diagram bar. \* $P < 0.05$ , \*\*\*\* $P < 10^{-5}$  (Student's *t*-test).

counterparts (Fig. 6B). This result is reinforced by the similar response of mitochondria in each CGN type when treated with all iGluR agonists NMDA and AMPA added together (Fig. 6C) or of glutamate-stimulated cortical neurons (Fig. S1B). We interpreted these results as reflecting the significantly higher  $Ca^{2+}$  entry in PrP-KO than in PrP-Tg neurons (Fig. 6A), but also a different endoplasmic reticulum (ER)  $Ca^{2+}$  discharge, possibly through channels responsive to metabotropic glutamate receptor (mGluR)-produced inositol 1,4,5-trisphosphate ( $IP_3$ ) (Ribeiro et al., 2010), given the close coupling between ER and mitochondrial membranes (Rizzuto et al., 1998; Rowland and Voeltz, 2012).

To understand the specific ER contribution to mitochondrial  $Ca^{2+}$ , CGNs were then treated with 3,5-dihydroxyphenylglycine (DHPG), a synthetic agonist of group I mGluRs (mGluR1 and mGluR5). This protocol (Fig. S4A, gray line and gray bar), or the addition of glutamate in the absence of external  $Ca^{2+}$  (data not shown), produced only a negligible mitochondrial  $Ca^{2+}$  uptake in PrP-Tg

CGNs, with no appreciable difference between PrP-Tg and PrP-KO CGNs (data not shown). A similar sluggish response was observed under depolarizing conditions (in the presence of 125 mM KCl, data not shown) to allow voltage-gated  $Ca^{2+}$  channels to deliver the external  $Ca^{2+}$  apparently necessary to stimulate phospholipase C under this condition (Masgrau et al., 2001). In contrast, cortical neurons effectively responded to DHPG (Fig. S4A, black line and black bar), as well as to glutamate in the absence of external  $Ca^{2+}$  (data not shown). The different response of CGNs and cortical neurons to DHPG prompted us to analyze their mGluR5 content. As expected, PrP-Tg and PrP-KO CGNs expressed extremely low amounts of this receptor, in contrast to the much higher mGluR5 abundance detected in cortical neurons (Fig. S4B).

#### PrP<sup>C</sup> downregulates CICR

In light of the results indicating that  $IP_3$ -sensitive channels contributed minimally to mitochondrial  $Ca^{2+}$  accumulation in

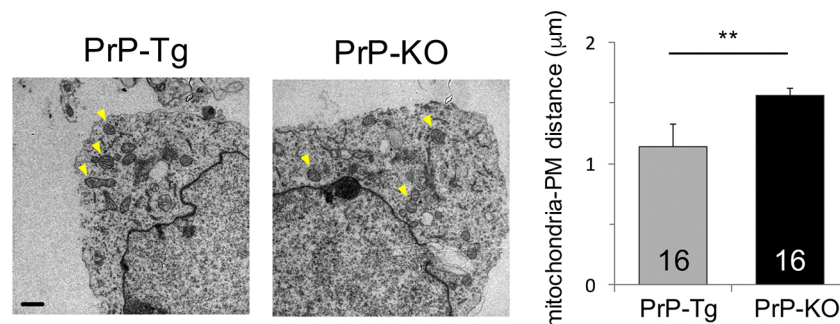


**Fig. 5. PrP-KO mitochondria are more distant from the PM than PrP-Tg mitochondria.** Ultra-thin (80 nm) CGN cross-sections were analyzed by transmission electron microscopy (TEM). Representative TEM micrographs from PrP-Tg and PrP-KO neurons are reported in the left panels, in which some mitochondria are indicated by yellow arrowheads. The bar diagram on the right reports the quantification of the mitochondria-PM distance, calculated as the average distance between the center of mitochondria and the closest rim of the PM, showing that the mitochondria-PM distance is higher in PrP-KO than in PrP-Tg CGNs. The analysis was carried out on a total of 16 randomly collected EM images for each CGNs genotype, comprising four technical replicates (i.e. different EM specimen) for each of the four performed biological replicates (i.e. different primary CGNs cultures); values are expressed as mean  $\pm$  s.e.m. Scale bar: 1  $\mu m$ . \*\* $P < 0.01$  (Student's *t*-test).

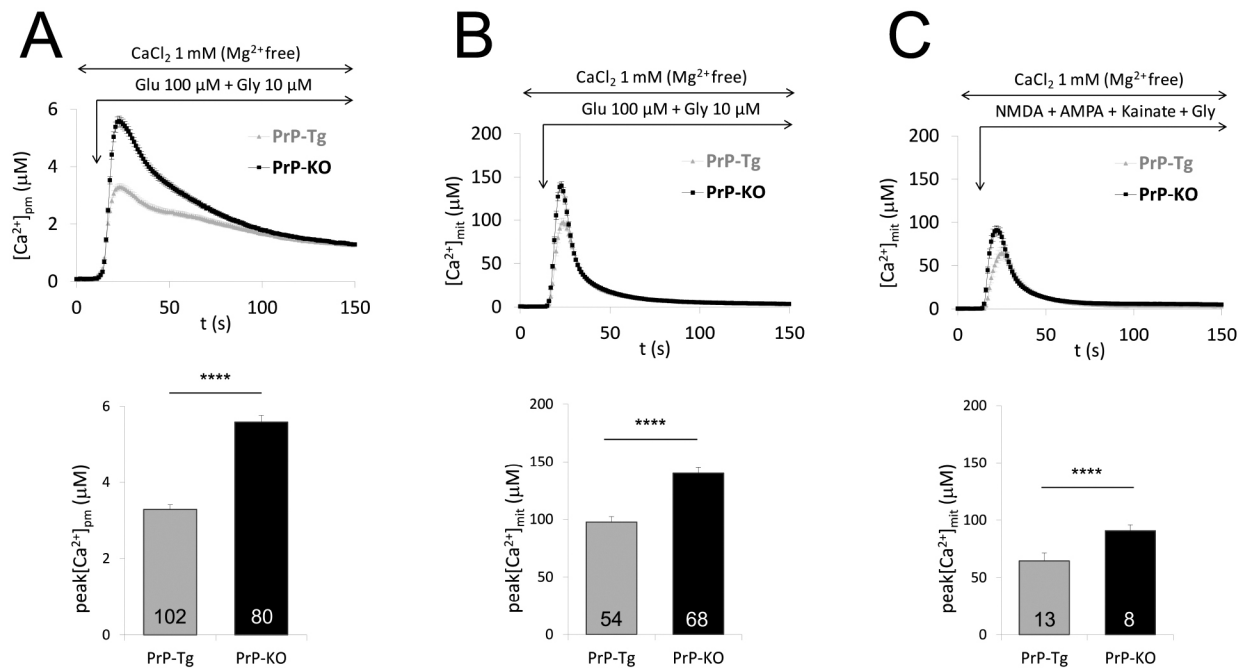


**Fig. 6. PrP<sup>C</sup> reduces cell Ca<sup>2+</sup> entry and mitochondrial Ca<sup>2+</sup> uptake in glutamate-stimulated CGNs.** CGNs were analyzed for Ca<sup>2+</sup> transients in PM subdomains (A) and the mitochondrial matrix (B) after stimulation with glutamate (Glu, in the absence of Mg<sup>2+</sup> and in the presence of Gly, as indicated), which activates all ionotropic and metabotropic receptors. As evident from the average kinetics of Ca<sup>2+</sup> transients (upper panels) and the corresponding Ca<sup>2+</sup> peak values (lower panels), PrP-KO CGNs displayed a higher level of Ca<sup>2+</sup> entry from the extracellular space and higher mitochondrial Ca<sup>2+</sup> uptake than PrP-Tg neurons. A similar difference in mitochondrial Ca<sup>2+</sup> transients was maintained when CGNs were treated with a mixture of all agonists to iGluRs (in the absence of Mg<sup>2+</sup> and in the presence of Gly) (C). Values are expressed as mean ± s.e.m., and the number of replicates (i.e. different coverslips from at least three primary CGNs cultures prepared on different days) is indicated inside each diagram bar. \*\*\*\**P* < 10<sup>-5</sup> (Student's *t*-test).

glutamate-stimulated CGNs, we considered whether CICR could be responsible for the higher Ca<sup>2+</sup> transients observed in PrP-KO mitochondria. CICR is mediated by ryanodine receptor (RyR) channels after activation by external Ca<sup>2+</sup> entry, and plays an important role in excitable cells by discharging Ca<sup>2+</sup> from the ER/sarcoplasmic reticulum, promoting mitochondrial uptake and spreading the Ca<sup>2+</sup> signal throughout the cell (Rizzuto et al., 1998; Berridge, 2002, 2006; Rowland and Voeltz, 2012).

After assessing that equal (type 2) RyR amounts were present in both CGN genotypes (data not shown), glutamate-induced mitochondrial Ca<sup>2+</sup> uptake was monitored in the presence of ryanodine concentrations (50 μM) that are known to inhibit RyRs (Sutko et al., 1997). As reported in Fig. 7, ryanodine slightly reduced mitochondrial Ca<sup>2+</sup> uptake in PrP-Tg CGNs (compare gray lines and bars of Fig. 7A and Fig. 7B) while the strong action on PrP-KO neurons (compare black lines and bars of panels Fig. 7A and Fig. 7B) nullified the difference in Ca<sup>2+</sup> peaks that was observed in untreated CGNs. Collectively, these results demonstrate that, by depressing Ca<sup>2+</sup> entry, PrP<sup>C</sup> safeguards CGNs from CICR-mediated mitochondrial Ca<sup>2+</sup> overload.

## DISCUSSION

The present work aimed at detailing the suggested involvement of PrP<sup>C</sup> in neuronal Ca<sup>2+</sup> homeostasis (Sorgato and Bertoli, 2009; Stys et al., 2012; Peggion et al., 2017) by examining the possible influence of PrP<sup>C</sup> on iGluR-mediated Ca<sup>2+</sup> entry and glutamate-induced Ca<sup>2+</sup> release from the ER. Recombinant AEQs were employed to compare local Ca<sup>2+</sup> movements in primary neurons expressing, or not expressing, PrP<sup>C</sup>. Notably, the sub-PM localization of AEQpm strategically enables the probe to sense iGluR-mediated transient Ca<sup>2+</sup> hot spots (Filadi and Pozzan, 2015),

while the AEQmit position in the mitochondrial matrix provides direct information on mitochondrial Ca<sup>2+</sup> fluxes. Exploitation of AEQs, apparently never employed before to follow PrP<sup>C</sup>-dependent GluR-induced Ca<sup>2+</sup> fluxes, helps to identify the precise sites at which PrP<sup>C</sup> regulates neuronal Ca<sup>2+</sup> homeostasis under physiological, and possibly pathological, conditions.

Combination of the above approaches demonstrated that PrP<sup>C</sup> prevents NMDAR-mediated Ca<sup>2+</sup> overflow in CGNs and in cortical neurons, in accord with data on hippocampal paradigms (Khosravani et al., 2008a; You et al., 2012). However, we could demonstrate that, in CGNs, PrP<sup>C</sup> downregulates AMPARs, and likely also kainateRs, suggesting that the control of all iGluRs underlies PrP<sup>C</sup> protective functions. Importantly, the insensitivity of voltage-gated Ca<sup>2+</sup> channels (VGCCs) to PrP<sup>C</sup> (De Mario et al., 2015) excluded the possibility that they could contribute to the different Ca<sup>2+</sup> fluxes detected in the present work. Furthermore, we have also found that AMPA-induced Ca<sup>2+</sup> fluxes were insensitive to the addition of nifedipine (data not shown), an inhibitor of L-type VGCC mostly present in CGNs (Schramm et al., 1999).

In trying to identify the pathway(s) by which PrP<sup>C</sup> controls iGluR activity, we considered the involvement of kinases such as Fyn and CaMKII, which are known to modulate channel activity and/or trafficking of NMDARs and AMPARs (Chen and Roche, 2007; Lu and Roche, 2012; Lussier et al., 2015), and are also functionally linked to PrP<sup>C</sup> (Mouillet-Richard et al., 2000; Schneider et al., 2003; Monnet et al., 2004; Beraldo et al., 2011; Um et al., 2013; Raka et al., 2015; Haas et al., 2016). However, because our experimental setup was operationally unsuited to mimic the complex parameters, including the actual and past activity of neurons, which may ultimately control the activation of the enzymes and their downstream effects (Henley and Wilkinson, 2013; Diering et al.,



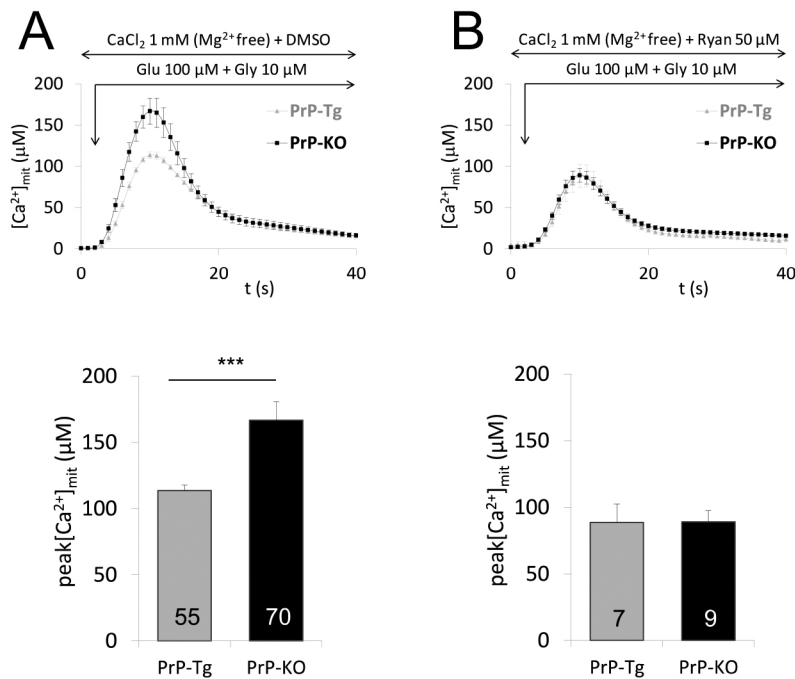


**Fig. 7. PrP<sup>C</sup> regulates Ca<sup>2+</sup>-induced Ca<sup>2+</sup>-release in CGNs.** CGNs were analyzed for mitochondrial Ca<sup>2+</sup> transients following stimulation with glutamate in the absence [but with the vehicle DMSO 0.2% (v/v)] (A), or in the presence of ryanodine (Ryan, 50  $\mu M$ , a concentration inhibitory to RyRs) (B). The average kinetics of local Ca<sup>2+</sup> transients, reported in the upper panels, and the corresponding Ca<sup>2+</sup> peaks of the lower bar diagrams, show that RyR inhibition totally abrogates the difference observed in controls, indicating that CICR was responsible for the higher mitochondrial Ca<sup>2+</sup> uptake in PrP-KO neurons compared to that in the PrP-Tg counterpart. Values are expressed as mean  $\pm$  s.e.m., and the number of replicates (i.e. different coverslips from at least three primary CGNs cultures prepared on different days) is indicated inside each diagram bar. \*\*\* $P < 0.001$  (Student's *t*-test).

2016), we analyzed whether PrP<sup>C</sup> could affect the basal state of the enzymes – in analogy to our recently described PrP-dependent downregulation of Fyn (De Mario et al., 2015) – and some downstream targets.

Regarding NMDARs, the PrP<sup>C</sup>–Fyn link was particularly attractive because several tyrosine residues serve as Fyn targets and because phosphorylation of GluN2B Tyr1472 controls the surface density of NMDARs (reviewed in Lussier et al., 2015). Interestingly, the binding of Alzheimer's disease (AD)-related A $\beta$  oligomers to PrP<sup>C</sup> hampers this process through the mediation of mGluR5, and provokes synapse loss (Um et al., 2012, 2013). Here, blocking Fyn activity with either the SFK-specific saracatinib or the less-specific PP2 kinase inhibitor resulted in a lower NMDAR-induced PM Ca<sup>2+</sup> peak but did not abrogate the peak difference between the two CGN genotypes. This evidence, and the finding that PP2 was more effective than saracatinib in reducing NMDA-evoked Ca<sup>2+</sup> entry, underscores that phosphorylation by SFK and non-SFK members may, indeed, upregulate NMDARs, but definitively exclude that the different PM Ca<sup>2+</sup> peak observed in PrP-Tg and PrP-KO CGNs relies on the PrP-dependent regulation of NMDAR residency at the PM through Fyn.

After excluding the possibility that CaMKII was involved in the synaptic expression of CGN NMDARs (O'Leary et al., 2011; Chen and Roche, 2007) because of the identical basal activation of the enzyme detected in both CGN genotypes, we considered whether PrP<sup>C</sup> could prevent NMDAR-mediated Ca<sup>2+</sup> overload by favoring the receptor desensitization process, particularly under a prolonged agonist exposure (You et al., 2012; Stys et al., 2012). Explicitly, it has been proposed that, by complexing with ambient copper ions [with variable (femto/nano molar) affinity at N-terminal sites (for a review see Viles et al., 2008; Grande-Aztatzi et al., 2013)] and interacting with the glycine-binding GluN1 subunit, PrP<sup>C</sup> lowers the affinity for the co-agonist glycine, which otherwise would reduce – in a dose-dependent manner – NMDAR desensitization and protract channel opening (Mayer et al., 1989; Vyklický et al., 1990). Examination of the KRB-based media (employed for Ca<sup>2+</sup> measurements) by using inductively coupled plasma atomic emission spectroscopy (Di Noto et al., 1995) revealed a contamination by (total) copper ions of

~500 nM. Therefore, one could tentatively speculate that this copper ion concentration could still enable PrP<sup>C</sup> to counteract the effect of non-physiological (high) concentrations of glycine, ultimately resulting in attenuation of NMDA-driven Ca<sup>2+</sup> influx.

To our knowledge, less information, if any, is available for the PrP-dependent modulation of AMPARs we observed in CGNs. In fact, limitation of AMPA-stimulated Ca<sup>2+</sup> fluxes we observed in CGNs. In fact, limitation of AMPA-stimulated Ca<sup>2+</sup> fluxes by PrP<sup>C</sup> contrasts with previous data indicating that AMPAR currents, or AMPA-mediated response to LTD stimuli, are independent of PrP<sup>C</sup> (Khosravani et al., 2008a,b). Tentative explanations for this discrepancy may rely on the different experimental settings, or on the type and *in vitro* developmental stage of the examined paradigms, given that the functional composition of iGluRs may vary in different neurons and/or during development (Henley and Wilkinson, 2013; Paoletti et al., 2013). Whatever the reason, our data on CGNs not only enrich the list of PrP<sup>C</sup>-regulated receptors and channels (Rangel et al., 2007; Beraldo et al., 2010, 2011; Carulla et al., 2011; Lazzari et al., 2011; Watt et al., 2012; De Mario et al., 2015; Fan et al., 2016), but – specifically to the crucial involvement of AMPARs in LTP and LTD (Henley and Wilkinson, 2013) – cast further significance on the involvement of PrP<sup>C</sup> in synaptic plasticity (as hypothesized long ago, for example, by Collinge et al., 1994).

Regarding the mechanism enabling PrP<sup>C</sup> to regulate AMPARs, no difference in the phosphorylation of Ser831 at the AMPAR GluR1 subunit was observed in the two CGN genotypes under unstimulated conditions (congruent with their similar CaMKII basal activity). Conversely, we found that PrP<sup>C</sup> acted negatively on the PKA-dependent phosphorylation of GluR1 Ser845, possibly because the observed basal downregulation of ERK1/2 by PrP<sup>C</sup> (Fig. S2D) limits ERK1/2-mediated inhibition of PDE (Song et al., 2013). The likely lower cAMP amounts produced in the presence of PrP<sup>C</sup> compared to when PrP<sup>C</sup> is absent (see Chiarini et al., 2002) results, therefore, in less active PKA, consistent with our findings that a reduced phosphorylation of GluR1 Ser845 leads to lower amounts of GluR1 (and GluR1-containing AMPARs) at the neuronal surface of PrP-expressing neurons (Fig. 3).

Of interest is that use of a targeted Ca<sup>2+</sup> probe allowed us to precisely monitor Ca<sup>2+</sup> fluxes in the mitochondrial matrix, thus

providing the novel information that PrP<sup>C</sup> may safeguard mitochondria from glutamate-induced dangerous Ca<sup>2+</sup> load. PrP<sup>C</sup> accomplishes this task by downregulating iGluRs in such a way that the generated Ca<sup>2+</sup> influx seems almost incapable of activating CICR in PrP-Tg CGNs. Interestingly, CICR is apparently the major route exploited by CGNs to discharge ER Ca<sup>2+</sup>, given that these neurons did not respond to DHPG, which activates IP<sub>3</sub>-producing group 1 mGluRs.

Taken together, the presented data highlight that PrP<sup>C</sup> controls Ca<sup>2+</sup> homeostasis in different cell compartments of neurons following exposure to physiological glutamate concentrations. Glutamate is the major excitatory neurotransmitter responsible for learning and memory (Malenka and Bear, 2004; Henley and Wilkinson, 2013), which are based on cytosolic Ca<sup>2+</sup> rise consequent to iGluR activity, or glutamate-mediated Ca<sup>2+</sup> discharge from internal stores. Clearly, regulation of all GluRs must be extremely precise, and the present work shows that PrP<sup>C</sup> contributes to the cell apparatus preventing glutamate excitotoxicity, and excessive Ca<sup>2+</sup> load therein, which could switch a beneficial signal into one disrupting synapse functions. Of relevance in this scenario, is the demonstration that the influence of PrP<sup>C</sup> extends from the PM to mitochondrial metabolism, because attenuation of the activity of all iGluRs by PrP<sup>C</sup> limits CICR and mitochondrial Ca<sup>2+</sup> uptake. In this way, PrP<sup>C</sup> could preclude dysregulation of key functional aspects of mitochondria, including the permeability of the inner membrane, which guarantees the functional integrity of the organelle (Bernardi et al., 2015).

This notion is of particular importance in the context of neurodegenerative processes involving glutamate and PrP<sup>C</sup>. Indeed, impaired glutamate signaling is a major player in neurodegenerative disorders (Lewerenz and Maher, 2015), while PrP<sup>C</sup> not only causes fatal prion diseases following conformational misfolding (Prusiner, 1998) but could also serve as a high-affinity receptor for both prions (Resenberger et al., 2011) and AD-causing Aβ oligomers (Laurén et al., 2009). One can envisage, therefore, that the structure and/or the function of PrP<sup>C</sup> are compromised after forming complexes with misfolded oligomers, and that, as mimicked in part by our PrP-KO model, diversion from the native protective function of PrP<sup>C</sup> contributes to neuronal pathogenesis.

Another interesting observation of this work, which also deserves further elucidation, is the apparent capability of PrP<sup>C</sup> to control the distribution of mitochondria in CGNs in such a way that mitochondria of PrP-KO CGNs are more distant from the PM than in PrP-Tg neurons. This fact could explain why mitochondria of PrP-KO neurons took up less Ca<sup>2+</sup> than PrP-Tg CGNs after activation of a single iGluR type (NMDAR or AMPAR) (Fig. 4), although more abundant extracellular Ca<sup>2+</sup> entry was detected in the former neuronal type (Fig. 1). Instead, when all iGluRs were stimulated by glutamate, the resulting increased total Ca<sup>2+</sup> flux (Fig. 6A) activated CICR to a much larger extent in PrP-KO than in PrP-Tg CGNs, which led to a higher mitochondrial Ca<sup>2+</sup> uptake (Fig. 6B and Fig. 7) despite the larger mitochondria–PM distance. Along this line, one might assume that inhibition of CICR by ryanodine resulted in a lower mitochondrial Ca<sup>2+</sup> uptake in PrP-KO than in PrP-Tg CGNs, as observed with NMDA or AMPA, alone. It is to be noted, however, that as glutamate in the presence of ryanodine elicited a much higher mitochondrial Ca<sup>2+</sup> transient than that recorded with iGluR agonists (compare Fig. 7B and Figs 4 and 6C), such an assumption is not necessarily well grounded.

Finally, our findings on PrP<sup>C</sup>-dependent mitochondria localization nicely fit in the framework of the alleged neuroprotective PrP<sup>C</sup> functions (see above). Indeed, pathological alterations of PrP<sup>C</sup>-related signaling are likely to result in a localization of mitochondria too far

from active synapses to allow delivery of the ATP amount necessary to satisfy the high energy demand of synapses.

## MATERIALS AND METHODS

### Animals

In this study, PrP-Tg and PrP-KO mice (lines Tg46 and F10, respectively) were used. Both strains were kindly provided by the MRC Prion Unit, London, UK. PrP-Tg (Tg46) mice served as control because the expression of PrP<sup>C</sup> in this strain was rescued over the PrP-KO (F10) genotype, thereby providing co-isogenic mouse lines (Mallucci et al., 2002). In addition, PrP-Tg mice express PrP<sup>C</sup> at the same level found in WT mice (Mallucci et al., 2002; Lazzari et al., 2011). Experiments were carried out in accordance with European and Italian (D.L. 26/2014) laws concerning the care and use of laboratory animals. The institution of the authors has been accredited for the use of mice for experimental purposes by the Italian Ministry of Health and by the Ethical Committee of the University of Padova (authorization no. 13/2012).

### Primary neuronal cultures

Primary cultures of CGNs and cortical neurons were prepared, cultured and transduced with lentiviral particles as previously described (De Mario et al., 2015), with minor modifications. Briefly, after seeding cells at the needed density (~9×10<sup>5</sup> and 6×10<sup>5</sup> onto poly-L-lysine-coated 13-mm coverslips for luminometer and immunocytochemistry assays, respectively; ~3×10<sup>6</sup> and 1.2×10<sup>6</sup> onto 35-mm poly-L-lysine-coated plates for western blotting and fluorescence/transmission electron microscopy assays, respectively), cells were maintained at 37°C in a humidified incubator with 5% CO<sub>2</sub>. Lentiviral particles were added to cells 24 h after plating, and after an additional 24 h cytosine arabinoside (0.04 mM for CGNs, and 0.01 mM for cortical neurons, Sigma) was supplemented to impede proliferation of non-neural cells. After a further 48 h (for CGNs), or 124 h (for cortical neurons), primary cultures were subjected to experimentation. As already proven for CGNs (Lazzari et al., 2011), the immunocytochemical analysis based on the neuronal (microtubule-associated protein 2; MAP2) and astrocytic (glial fibrillary acidic protein; GFAP) markers, revealed that primary cortical neurons were >97% pure (data not shown).

### Construction of lentiviral vectors for AEQs

To measure Ca<sup>2+</sup> transients in specific neuronal compartments, lentiviral vectors encoding AEQpm, AEQcyt or AEQmit were used (Lim et al., 2016). Lentiviral vectors for AEQpm and AEQmit were generated by using an AEQ mutant with reduced Ca<sup>2+</sup> affinity allowing measurements of Ca<sup>2+</sup> concentrations up to hundreds of micromolar, while a chimeric construct of WT AEQ was used to generate the lentiviral vector for AEQcyt (Lim et al., 2016). The expression and correct cellular localization of AEQs were determined by immunocytochemistry approaches (De Mario et al., 2015).

### Measurements of local Ca<sup>2+</sup> fluxes

To measure Ca<sup>2+</sup> transients in the cytosolic domains proximal to the PM ([Ca<sup>2+</sup>]<sub>pm</sub>), the cytosol ([Ca<sup>2+</sup>]<sub>cyt</sub>) and the mitochondrial matrix ([Ca<sup>2+</sup>]<sub>mit</sub>) following stimulation of iGluRs or mGluRs, neurons were first incubated (1 h, 37°C, 5% CO<sub>2</sub>) in Krebs-Ringer buffer (KRB; 125 mM NaCl, 5 mM KCl, 1 mM KH<sub>2</sub>PO<sub>4</sub>, 1 mM MgSO<sub>4</sub>, 5.5 mM glucose, 20 mM HEPES, pH 7.4) containing CaCl<sub>2</sub> (1 mM, for AEQcyt and AEQmit) or EGTA (100 μM, for AEQpm), and the AEQ cofactor coelenterazine (5 μM, Santa Cruz Biotechnology, cat. no. sc-205904). After transferring coverslips to the thermostatted chamber of a purpose-built luminometer, perfusion of neurons varied according to the envisaged GluR stimulation. That is, if all iGluRs were the simultaneous target, neurons were perfused (1 min) with Mg<sup>2+</sup>-free (Ruppersberg et al., 1994) KRB (containing 1 mM CaCl<sub>2</sub>), and then with either glutamate (100 μM, Sigma) plus the co-agonist glycine (10 μM, Sigma), or a mixture of NMDA (50 μM, Sigma), AMPA (100 μM, Tocris) and kainate (30 μM, Tocris) plus glycine (10 μM); in the case of a single iGluR activation, the specific agonist, namely NMDA (plus 10 μM glycine), AMPA or kainate (all at the above concentrations) was added (KRB was Mg<sup>2+</sup> free only with NMDA); when activating mGluRs specifically, either DHPG (100 μM, Tocris) or glutamate in CaCl<sub>2</sub>-free KRB was used. If needed, the specific-SFK inhibitor saracatinib (5 μM,



Santa Cruz Biotechnology, cat. no. sc-364607) or the less-specific PP2 (10  $\mu$ M Tocris, cat. no. 1407), both diluted in 0.01% (v/v) dimethyl sulfoxide (DMSO), was present throughout the experiment starting from the addition of coelenterazine, while ryanodine [50  $\mu$ M in 0.2% (v/v) DMSO, Tocris], at inhibitory concentrations to RyRs, was present from the  $Mg^{2+}$ -free perfusion step.

AEQ light emission was recorded using an in-house built luminometer, equipped with a low-noise photo-multiplier coupled with an analog-to-digital converter to a computer-assisted acquisition system (Ottolini et al., 2014), at a 1 Hz sampling rate. At the end of each recording, cells were perfused with KRB containing digitonin (50  $\mu$ M, Sigma) and a saturating  $Ca^{2+}$  concentration (10 mM), allowing the calibration of the recorded light signal to the total AEQ content. The conversion of the light signal into  $Ca^{2+}$  concentration was carried out using the algorithm and the custom-made software previously described (Brini et al., 1995; Montero et al., 1995).

### Measurement of mitochondrial membrane potential

Tetramethylrhodamine methyl ester (TMRM,  $\lambda_{exc}=548$  nm,  $\lambda_{em}=574$  nm, Molecular Probes) was employed to measure  $\Delta\psi_m$  of CGNs. To this end, experiments were carried out under basal conditions (i.e. the conditions used for detecting  $Ca^{2+}$  fluxes in the organelle but in the absence of stimuli). TMRM is permeable to the PM and, being a cation, it accumulates electrophoretically into the matrix of respiring mitochondria (Scaduto and Grotyohann, 1999). Coverslip images were collected using an inverted microscope (Olympus IMT-2) equipped with a (75W) xenon lamp, a 16-bit digital CCD camera (cooled by a Miromax system, Princeton Instruments), a 40 $\times$  oil objective, and appropriate excitation and emission filters. Several fields were acquired from each coverslip before and after the addition of trifluorocarbonylcyanide phenylhydrazide (FCCP) (5  $\mu$ M, Sigma), which, by collapsing  $\Delta\psi_m$ , induces the release of TMRM from mitochondria. Images were analyzed with Image J software. Fluorescence density was measured in mitochondria-rich regions and calculated as the difference between the mean fluorescence density detected before and after FCCP addition. TMRM fluorescence density was then reported as percentage of the PrP-Tg mean value.

### Transmission electron microscopy

We used TEM to quantify mitochondria in CGNs and their distance from the PM. CGNs were fixed in glutaraldehyde [3.9% (w/v) in a sodium cacodylate buffer, pH 7.4], and embedded in Epon 812 resin. Ultra-thin (80 nm) cross-sections were cut with a microtome (Ultratome V, LKB), mounted on copper grids, contrasted with uranyl acetate (1%) and lead citrate (1%), and examined at a transmission electron microscope (Tecnai G2, FEI) operating at 100 kV. Images were acquired with a digital camera (F114, Tvips) and a dedicated software (TIA, FEI), and the density of mitochondria per area units in soma and dendrites was calculated using the Image J software. The mitochondria-PM distance was estimated (using the latter software) as the shortest distance between the center of each mitochondrion and the rim of the PM. To guarantee that mitochondria were randomly selected for statistical analyses, 4 different cell preparations from each of the used 4 independent cultures were analyzed by TEM for either PrP-tG or PrP-KO genotype. At least 70 mitochondria were generally measured in a single cell preparation, and data were reported as the mean of the 16 replicates for an individual CGN genotype.

### Western blotting analysis

CGNs were incubated (1 h, 37°C, 5%  $CO_2$ ) in KRB supplemented with  $CaCl_2$  (1 mM), and subsequently lysed in a buffer containing 10% (w/v) glycerol, 2% (w/v) sodium dodecyl sulfate (SDS), 62.5 mM Tris-HCl (pH 6.8), 1.8 M urea, 5 mM  $Na_3VO_4$ , protease and phosphatase inhibitor cocktails (Roche). After determining the protein concentration (Total Protein Kit, micro Lowry, Peterson's modification, Sigma), lysates were adjusted to an equal protein concentration using reducing (50 mM dithiothreitol) Laemmli sample buffer. After boiling (5 min), lysates were subjected to SDS-PAGE [10% (w/v) acrylamide-N,N'-methylenebisacrylamide (37.5:1)] and electroblotted onto nitrocellulose membranes (0.45  $\mu$ m pore size, Biorad) to detect SDHA, or onto polyvinylidene difluoride (PVDF) membranes (0.45  $\mu$ m pore

size, Millipore) to detect MCU, mGluR5 that was phosphorylated or not (on Ser831 or Ser845), the GluR1 subunit of AMPARs phosphorylated or not (on Thr202/Tyr204), ERK1/2, and (auto) phosphorylated (on Thr286) CaMKII. To verify equal loading and transfer, nitrocellulose membranes were stained with Ponceau Red, while Coomassie Blue was used to stain PVDF membranes. After de-staining, membranes were incubated (1 h, room temperature) with a blocking solution [Tris-buffered saline added with 0.1% (w/v) Tween-20 (TBS-T) and 3% (w/v) bovine serum albumin (BSA)], followed by incubation (overnight, 4°C) with one of the following primary rabbit polyclonal antibodies (pAbs) (dilution in parenthesis): anti-SDHA [Sigma cat. no. SAB1100429; 1:1000 in BSA 3% (w/v) added to TBS-T]; anti-MCU [i.e. to the channel-forming MCU subunit, Sigma cat. no. HPA016480; 1:1000 in milk 5% (w/v) added to TBS-T]; anti-mGluR5 [Millipore cat. no. ab5675; 1:2000 in BSA 1% (w/v) added to TBS-T]; anti-GluR1 [Millipore cat. no. ab1504; 1:1000 in BSA 3% (w/v) added to TBS-T]; anti-phosphorylated CaMKII (on Thr286) [Cell Signaling Tech. cat. no. 3361; 1:500 in milk 5% (w/v) added to TBS-T], the correct targeting of which was verified under depolarized conditions that maximally activated CaMKII by  $Ca^{2+}$  (KCl being raised to 145 mM 2 min before cell lysis); anti-phosphorylated GluR1 (on Ser831) [Millipore cat. n. ab5847; 1:1000 in milk 5% (w/v) added to TBS-T]; anti-phosphorylated GluR1 (on Ser845) [Santa Cruz Biotechnology cat. no. sc-135699; 1:500 in BSA 3% (w/v) added TBS-T]; anti-ERK1/2 [Cell Signaling Tech., cat. no. 9102; 1:1000 in BSA 3% (w/v) added to TBS-T]. Detection of phosphorylated ERK1/2 was performed using a primary mouse monoclonal Ab [Cell Signaling Tech. cat. no. 9106; 1:1000 in BSA 3% (w/v) added to TBS-T]. After three washing steps (10 min each in TBS-T), membranes were incubated (1 h, room temperature) with a horseradish peroxidase-conjugated anti-rabbit-IgG, or anti-mouse-IgG secondary Ab (Santa Cruz Biotechnology cat. no. sc-2004/2005). Immunoreactive bands were visualized and digitalized by means of a digital Kodak Image Station, using an enhanced chemiluminescence reagent kit (Millipore). For densitometric analyses, band intensities were normalized to the optical density of the corresponding lanes stained with Ponceau Red or Coomassie Blue (Welinder and Ekblad, 2011). When analyzing GluR1 or ERK1/2 phosphorylation, samples were run in parallel in the same gel, and then probed with either the Ab to the phosphorylated form or to the total protein; the band intensity of the phosphorylated form was finally normalized to that of the corresponding signal of total GluR1 or ERK1/2. All data are reported as fraction of the mean values of PrP-Tg samples.

### Cell surface biotinylation

At 96 h after plating, CGNs were washed twice with ice-cold KRB supplemented with 1 mM  $CaCl_2$ , and gently shaken (1 h, 4°C) in KRB containing a membrane-impermeable biotin derivative (EZ-Link Sulfo-NHS-LC biotin, Thermo Scientific, cat. no. 21335; 0.75 mg  $ml^{-1}$ ). Unbound biotin was removed by extensive washings of neurons, first with ice-cold KRB, and then (three times) with ice-cold glycine (20 mM)-containing PBS. Cells were lysed using a lysis buffer containing 150 mM NaCl, 1 mM EDTA, 50 mM Tris-HCl (pH 7.4), 1% (v/v) Triton X-100 and a protease inhibitors cocktail (Roche); cell lysates [300  $\mu$ g of total proteins, determined by a bicinchoninic acid-based protein assay kit (Thermo Scientific)] were centrifuged (16,000 g, 15 min, 4°C), and the supernatant was incubated (overnight, 4°C) with streptavidin-coated magnetic beads (Thermo Scientific, cat. no. 88816). After two washings in lysis buffer, beads were collected using a magnetic rack (SureBeads, BioRad). After elution with Laemmli sample buffer containing 200 mM dithiothreitol as reducing agent, biotinylated proteins were separated by SDS-PAGE (4–15% gradient acrylamide-N,N'-methylenebisacrylamide, PROTEAN TGX precast electrophoresis gels, Bio-Rad), electroblotted onto PVDF membranes and immunoprobed with the anti-GluR1 Ab (see above). To determine total neuronal GluR1 amounts, lysates (10  $\mu$ g) were analyzed as hitherto described, except for omitting the addition of streptavidin-coated magnetic beads. For densitometric analyses, band intensities were normalized to the optical density of the corresponding Coomassie Blue-stained lanes, and the band intensity of the biotinylated GluR1 form was normalized to that of the corresponding total GluR1 signal. Data are reported as fraction of the mean values of PrP-Tg samples.

## Statistical analysis

Values are reported as mean±s.e.m. Data analysis was performed as described in detail in Lazzari et al. (2011). Statistics was based on two-sample Student's *t*-test, with *P* < 0.05 being considered statistically significant (\**P* < 0.05, \*\**P* < 0.01, \*\*\**P* < 0.001, \*\*\*\**P* < 10<sup>−5</sup>).

## Acknowledgements

The authors are grateful to Dr Ketì Vezzù (Section of Chemistry for Technology, Dept. of Industrial Engineering, Padova University, Italy) for estimating copper ion levels by inductively-coupled plasma atomic emission spectroscopy, Dr Fiorella Tonello (CNR Institute of Neuroscience, Padova University) for expert suggestions on cell biotinylation procedures and the Electron Microscopy Service, Dept. of Biology, Padova University.

## Competing interests

The authors declare no competing or financial interests.

## Author contributions

Conceptualization: A.D.M., C.P., M.G., A.B., M.C.S.; Methodology: A.D.M., C.P., D.L., M.L.M., A.C., A.B.; Validation: A.D.M., A.B., C.P.; Formal analysis: A.D.M., C.P., A.B.; Investigation: A.D.M., C.P., M.L.M., F.V., A.C.; Resources: A.B., M.L.M.; Data curation: A.D.M., C.P., A.B.; Writing - original draft: A.D.M., C.P., A.B., M.C.S.; Writing - review & editing: A.B., M.C.S.; Supervision: A.B., M.C.S.; Project administration: A.B., M.C.S.; Funding acquisition: A.B., M.C.S.

## Funding

This work was supported by the Università degli Studi di Padova (University of Padova) (PRAT CPDA121988/12 to M.C.S.; PRAT CPDA158035/15 to A.B.).

## Supplementary information

Supplementary information available online at <http://jcs.biologists.org/lookup/doi/10.1242/jcs.196972.supplemental>

## References

- Banke, T. G., Bowie, D., Lee, H., Haganir, R. L., Schousboe, A. and Traynelis, S. F. (2000). Control of GluR1 AMPA receptor function by cAMP-dependent protein kinase. *J. Neurosci.* **20**, 89–102.
- Barria, A., Muller, D., Derkach, V., Griffith, L. C. and Soderling, T. R. (1997). Regulatory phosphorylation of AMPA-type glutamate receptors by CaM-KII during long-term potentiation. *Science* **276**, 2042–2045.
- Beraldo, F. H., Arantes, C. P., Santos, T. G., Queiroz, N. G. T., Young, K., Rylett, R. J., Markus, R. P., Prado, M. A. M. and Martins, V. R. (2010). Role of alpha7 nicotinic acetylcholine receptor in calcium signaling induced by prion protein interaction with stress-inducible protein 1. *J. Biol. Chem.* **285**, 36542–36550.
- Beraldo, F. H., Arantes, C. P., Santos, T. G., Machado, C. F., Roffe, M., Hajj, G. N., Lee, K. S., Magalhães, A. C., Caetano, F. A., Mancini, G. L. et al. (2011). Metabotropic glutamate receptors transduce signals for neurite outgrowth after binding of the prion protein to laminin  $\gamma$ 1 chain. *FASEB J.* **25**, 265–279.
- Bernardi, P., Rasola, A., Forte, M. and Lippe, G. (2015). The Mitochondrial Permeability Transition Pore: Channel Formation by F-ATP Synthase, Integration in Signal Transduction, and Role in Pathophysiology. *Physiol. Rev.* **95**, 1111–1155.
- Berridge, M. J. (2002). The endoplasmic reticulum: a multifunctional signaling organelle. *Cell Calcium* **32**, 235–249.
- Berridge, M. J. (2006). Calcium microdomains: organization and function. *Cell Calcium* **40**, 405–412.
- Blackstone, C., Murphy, T. H., Moss, S. J., Baraban, J. M. and Haganir, R. L. (1994). Cyclic AMP and synaptic activity-dependent phosphorylation of AMPA-preferring glutamate receptors. *J. Neurosci.* **14**, 7585–7593.
- Brini, M., Marsault, R., Bastianutto, C., Alvarez, J., Pozzan, T. and Rizzuto, R. (1995). Transfected aequorin in the measurement of cytosolic Ca<sup>2+</sup> concentration ([Ca<sup>2+</sup>]<sub>i</sub>). A critical evaluation. *J. Biol. Chem.* **28**, 9896–9903.
- Carulla, P., Brihián, A., Rangel, A., Gavín, R., Ferrer, I., Caelles, C., del Río, J. A. and Llorens, F. (2011). Neuroprotective role of PrP<sup>C</sup> against kainate-induced epileptic seizures and cell death depends on the modulation of JNK3 activation by GluR6/7-PSD-95 binding. *Mol. Biol. Cell.* **22**, 3041–3054.
- Chen, B. S. and Roche, K. W. (2007). Regulation of NMDA receptors by phosphorylation. *Neuropharmacology* **533**, 62–68.
- Chiarini, L. B., Freitas, A. R. O., Zanata, S. M., Brentani, R. R., Martins, V. R. and Linden, R. (2002). Cellular prion protein transduces neuroprotective signals. *EMBO J.* **21**, 3317–3326.
- Collinge, J., Whittington, M. A., Sidle, K. C., Smith, C. J., Palmer, M. S., Clarke, A. R. and Jefferys, J. G. (1994). Prion protein is necessary for normal synaptic function. *Nature* **370**, 295–297.
- Criado, J. R., Sánchez-Alavez, M., Conti, B., Giacchino, J. L., Wills, D. N., Henriksen, S. J., Race, R., Manson, J. C., Chesebro, B. and Oldstone, M. B. A. (2005). Mice devoid of prion protein have cognitive deficits that are rescued by reconstitution of PrP in neurons. *Neurobiol. Dis.* **19**, 255–265.
- De Mario, A., Castellani, A., Peggion, C., Massimino, M. L., Lim, D., Hill, A. F., Sorgato, M. C. and Bertoli, A. (2015). The prion protein constitutively controls neuronal store-operated Ca<sup>2+</sup> entry through Fyn kinase. *Front. Cell. Neurosci.* **9**, 416.
- Diering, G. H., Heo, S., Hussain, N. K., Liu, B. and Haganir, R. L. (2016). Extensive phosphorylation of AMPA receptors in neurons. *Proc. Natl. Acad. Sci. USA* **113**, E4920–E4927.
- Di Noto, V., Ni, D., Dalla Via, L., Scomazzon, F. and Vidali, M. (1995). Determination of platinum in human blood using inductively coupled plasma atomic emission spectrometry with an ultrasonic nebulizer. *Analyst* **6**, 1669–1673.
- Fan, J., Stenkowski, P. L., Gandini, M. A., Black, S. A., Zhang, Z., Souza, I. A., Chen, L. and Zamponi, G. W. (2016). Reduced hyperpolarization-activated current contributes to enhanced intrinsic excitability in cultured hippocampal neurons from PrP<sup>C</sup> mice. *Front. Cell. Neurosci.* **10**, 74.
- Filadi, R. and Pozzan, T. (2015). Generation and functions of second messengers microdomains. *Cell Calcium* **58**, 405–414.
- Gadotti, V. M. and Zamponi, G. W. (2011). Cellular prion protein protects from inflammatory and neuropathic pain. *Mol. Pain* **7**, 59.
- Gadotti, V. M., Bonfield, S. P. and Zamponi, G. W. (2012). Depressive-like behaviour of mice lacking cellular prion protein. *Behav. Brain Res.* **227**, 319–323.
- Glancy, B. and Balaban, R. S. (2012). Role of mitochondrial Ca<sup>2+</sup> in the regulation of cellular energetics. *Biochemistry* **51**, 2959–2973.
- Grande-Aztatzi, R., Rivillas-Acevedo, L., Quintanar, L. and Vela, A. (2013). Structural models for Cu(II) bound to the fragment 92–96 of the human prion protein. *J. Phys. Chem. B* **117**, 789–799.
- Haas, L. T., Salazar, S. V., Kostylev, M. A., Um, J. W., Kaufman, A. C. and Strittmatter, S. M. (2016). Metabotropic glutamate receptor 5 couples cellular prion protein to intracellular signalling in Alzheimer's disease. *Brain* **139**, 526–546.
- Henley, J. M. and Wilkinson, K. A. (2013). AMPA receptor trafficking and the mechanisms underlying synaptic plasticity and cognitive aging. *Dialogues Clin. Neurosci.* **15**, 11–27.
- Haganir, R. L. and Nicoll, R. A. (2013). AMPARs and synaptic plasticity: the last 25 years. *Neuron* **80**, 704–717.
- Khosravani, H., Zhang, Y., Tsutsui, S., Hameed, S., Altier, C., Hamid, J., Chen, L., Villemaire, M., Ali, Z., Jirik, F. R. et al. (2008a). Prion protein attenuates excitotoxicity by inhibiting NMDA receptors. *J. Cell Biol.* **181**, 551–565.
- Khosravani, H., Zhang, Y. and Zamponi, G. W. (2008b). Cellular prion protein null mice display normal AMPA receptor mediated long term depression. *Prion* **2**, 48–50.
- Kristensen, A. S., Jenkins, M. A., Banke, T. G., Schousboe, A., Makino, Y., Johnson, R. C., Haganir, R. and Traynelis, S. F. (2011). Mechanism of Ca<sup>2+</sup>/calmodulin-dependent kinase II regulation of AMPA receptor gating. *Nat. Neurosci.* **14**, 727–735.
- Laurén, J., Gimbel, D. A., Nygaard, H. B., Gilbert, J. W. and Strittmatter, S. M. (2009). Cellular prion protein mediates impairment of synaptic plasticity by amyloid-beta oligomers. *Nature* **457**, 1128–1132.
- Lazzari, C., Peggion, C., Stella, R., Massimino, M. L., Lim, D., Bertoli, A. and Sorgato, M. C. (2011). Cellular prion protein is implicated in the regulation of local Ca<sup>2+</sup> movements in cerebellar granule neurons. *J. Neurochem.* **116**, 881–890.
- Lee, H.-K., Takamiya, K., He, K., Song, L. and Haganir, R. L. (2010). Specific roles of AMPA receptor subunit GluR1 (GluA1) phosphorylation sites in regulating synaptic plasticity in the CA1 region of hippocampus. *J. Neurophysiol.* **103**, 479–489.
- Lewerenz, J. and Maher, P. (2015). Chronic glutamate toxicity in neurodegenerative diseases—what is the evidence? *Front. Neurosci.* **9**, 469.
- Lim, D., Bertoli, A., Sorgato, M. C. and Moccia, F. (2016). Generation and usage of aequorin lentiviral vectors for Ca<sup>2+</sup> measurement in sub-cellular compartments of hard-to-transfect cells. *Cell Calcium* **59**, 228–239.
- Linden, R., Martins, V. R., Prado, M. A. M., Cammarota, M., Izquierdo, I. and Brentani, R. R. (2008). Physiology of the prion protein. *Physiol. Rev.* **88**, 673–728.
- Lu, W. and Roche, K. W. (2012). Posttranslational regulation of AMPA receptor trafficking and function. *Curr. Opin. Neurobiol.* **22**, 470–479.
- Lussier, M. P., Sanz-Clemente, A. and Roche, K. W. (2015). Dynamic regulation of N-Methyl-D-aspartate (NMDA) and  $\alpha$ -Amino-3-hydroxy-5-methyl-4-isoxazolepropionic acid (AMPA) receptors by posttranslational modifications. *J. Biol. Chem.* **290**, 28596–28603.
- Malenka, R. C. and Bear, M. F. (2004). LTP and LTD: an embarrassment of riches. *Neuron* **44**, 5–21.
- Mallucci, G. R., Ratté, S., Asante, E. A., Linehan, J., Gowland, I., Jefferys, J. G. R. and Collinge, J. (2002). Post-natal knockout of prion protein alters hippocampal CA1 properties, but does not result in neurodegeneration. *EMBO J.* **21**, 202–210.
- Masgrau, R., Servitja, J.-M., Young, K. W., Pardo, R., Sarri, E., Nahorski, S. R. and Picatoste, F. (2001). Characterization of the metabotropic glutamate receptors mediating phospholipase C activation and calcium release in cerebellar granule cells: calcium-dependence of the phospholipase C response. *Eur. J. Neurosci.* **13**, 248–256.
- Mayer, M. L., Vyklícký, L., Jr. and Clements, J. (1989). Regulation of NMDA receptor desensitization in mouse hippocampal neurons by glycine. *Nature* **338**, 425–427.

- Monnet, C., Gavard, J., Mège, R.-M. and Sobel, A. (2004). Clustering of cellular prion protein induces ERK1/2 and stathmin phosphorylation in GT1-7 neuronal cells. *FEBS Lett.* **576**, 114–118.
- Montero, M., Brini, M., Marsault, R., Alvarez, J., Sitia, R., Pozzan, T. and Rizzuto, R. (1995). Monitoring dynamic changes in free  $\text{Ca}^{2+}$  concentration in the endoplasmic reticulum of intact cells. *EMBO J.* **15**, 5467–5475.
- Mouillet-Richard, S., Ermonval, M., Chebassier, C., Laplanche, J. L., Lehmann, S., Launay, J. M. and Kellermann, O. (2000). Signal transduction through prion protein. *Science* **289**, 1925–1928.
- Murgia, M. and Rizzuto, R. (2015). Molecular diversity and pleiotropic role of the mitochondrial calcium uniporter. *Cell Calcium* **58**, 11–17.
- Nakazawa, T., Komai, S., Tezuka, T., Hisatsune, C., Umemori, H., Semba, K., Mishina, M., Manabe, T. and Yamamoto, T. (2001). Characterization of Fyn-mediated tyrosine phosphorylation sites on GluR epsilon 2 (NR2B) subunit of the N-methyl-D-aspartate receptor. *J. Biol. Chem.* **276**, 693–699.
- O'Leary, H., Liu, W. H., Rorabaugh, J. M., Coultrap, S. J. and Bayer, K. U. (2011). Nucleotides and phosphorylation bi-directionally modulate  $\text{Ca}^{2+}$ /calmodulin-dependent protein kinase II (CaMKII) binding to the N-methyl-D-aspartate (NMDA) receptor subunit GluN2B. *J. Biol. Chem.* **286**, 31272–31281.
- Ottolini, D., Cali, T. and Brini, M. (2014). Methods to measure intracellular  $\text{Ca}^{2+}$  fluxes with organelle-targeted aequorin-based probes. *Methods Enzymol.* **543**, 21–45.
- Ozawa, S., Kamiya, H. and Tsuzuki, K. (1998). Glutamate receptors in the mammalian central nervous system. *Prog. Neurobiol.* **5**, 581–618.
- Paoletti, P., Bellone, C. and Zhou, Q. (2013). NMDA receptor subunit diversity: impact on receptor properties, synaptic plasticity and disease. *Nat. Rev. Neurosci.* **14**, 383–400.
- Peggion, C., Bertoli, A. and Sorgato, M. C. (2011). Possible role for  $\text{Ca}^{2+}$  in the pathophysiology of the prion protein? *Biofactors* **37**, 241–249.
- Peggion, C., Bertoli, A. and Sorgato, M. C. (2017). Almost a century of prion protein(s): From pathology to physiology, and back to pathology. *Biochem. Biophys. Res. Commun.* **483**, 1148–1155.
- Powell, A. D., Toescu, E. C., Collinge, J. and Jefferys, J. G. R. (2008). Alterations in  $\text{Ca}^{2+}$  buffering in prion-null mice: association with reduced afterhyperpolarizations in CA1 hippocampal neurons. *J. Neurosci.* **28**, 3877–3886.
- Prusiner, S. B. (1998). Prions. *Proc. Natl. Acad. Sci. USA* **95**, 13363–13383.
- Raka, F., Di Sebastiano, A. R., Kulhawy, S. C., Ribeiro, F. M., Godin, C. M., Caetano, F. A., Angers, S. and Ferguson, S. S. (2015).  $\text{Ca}^{2+}$ /calmodulin-dependent protein kinase II interacts with group I metabotropic glutamate and facilitates receptor endocytosis and ERK1/2 signaling: role of  $\beta$ -amyloid. *Mol. Brain* **8**, 21.
- Rangel, A., Burgaya, F., Gavín, R., Soriano, E., Aguzzi, A. and del Río, J. A. (2007). Enhanced susceptibility of *Prnp*-deficient mice to kainate-induced seizures, neuronal apoptosis, and death: Role of AMPA/kainate receptors. *J. Neurosci. Res.* **85**, 2741–2755.
- Resenberger, U. K., Harmeier, A., Woerner, A. C., Goodman, J. L., Müller, V., Krishnan, R., Vabulas, R. M., Kretschmar, H. A., Lindquist, S., Hartl, F. U. et al. (2011). The cellular prion protein mediates neurotoxic signalling of  $\beta$ -sheet-rich conformers independent of prion replication. *EMBO J.* **30**, 2057–2070.
- Ribeiro, F. M., Paquet, M., Cregan, S. P. and Ferguson, S. S. G. (2010). Group I metabotropic glutamate receptor signalling and its implication in neurological disease. *CNS Neurol. Disord. Drug Targets* **9**, 574–595.
- Rizzuto, R., Pinton, P., Carrington, W., Fay, F. S., Fogarty, K. E., Lifshitz, L. M., Tuft, R. A. and Pozzan, T. (1998). Close contacts with the endoplasmic reticulum as determinants of mitochondrial  $\text{Ca}^{2+}$  responses. *Science* **280**, 1763–1766.
- Roucous, X., Gains, M. and LeBlanc, A. C. (2004). Neuroprotective functions of prion protein. *J. Neurosci. Res.* **75**, 153–161.
- Rowland, A. A. and Voeltz, G. K. (2012). Endoplasmic reticulum-mitochondria contacts: function of the junction. *Nat. Rev. Mol. Cell. Biol.* **13**, 607–625.
- Ruppersberg, J. P., Kitzing, v. E. and Schoepfer, R. (1994). The mechanism of magnesium block of NMDA receptors. *Semin. Neurosci.* **6**, 87–96.
- Scaduto, R. C., Jr. and Grotyhann, L. W. (1999). Measurement of mitochondrial membrane potential using fluorescent rhodamine derivatives. *Biophys. J.* **76**, 469–477.
- Schneider, B., Mutel, V., Pietri, M., Ermonval, M., Mouillet-Richard, S. and Kellermann, O. (2003). NADPH oxidase and extracellular regulated kinases 1/2 are targets of prion protein signaling in neuronal and non neuronal cells. *Proc. Natl. Acad. Sci. USA* **100**, 13326–13331.
- Schramm, M., Vajna, R., Pereverzev, A., Tottene, A., Klöckner, U., Pietrobon, D., Hescheler, J. and Schneider, T. (1999). Isoforms of  $\alpha 1\text{E}$  voltage-gated calcium channels in rat cerebellar granule cells: detection of major calcium channel  $\alpha 1$ -transcripts by reverse transcription-polymerase chain reaction. *Neuroscience* **92**, 565–575.
- Song, R. S., Massenburg, B., Wenderski, W., Jayaraman, V., Thompson, L. and Neves, S. R. (2013). ERK regulation of phosphodiesterase 4 enhances dopamine-stimulated AMPA receptor membrane insertion. *Proc. Natl. Acad. Sci. USA* **110**, 15437–15442.
- Sorgato, M. C. and Bertoli, A. (2009). From cell protection to death: may  $\text{Ca}^{2+}$  signals explain the chameleonic attributes of the mammalian prion protein? *Biochem. Biophys. Res. Commun.* **379**, 171–174.
- Spudich, R., Frigg, R., Kilic, E., Kilic, Ü., Oesch, B., Raeber, A., Bassetti, C. L. and Hermann, D. M. (2005). Aggravation of ischemic brain injury by prion protein deficiency: role of ERK-1/-2 and STAT-1. *Neurobiol. Dis.* **20**, 442–449.
- Stys, P. K., You, H. and Zamponi, G. W. (2012). Copper-dependent regulation of NMDA receptors by cellular prion protein: implications for neurodegenerative disorders. *J. Physiol.* **590**, 1357–1368.
- Sutko, J. L., Airey, J. A., Welch, W. and Ruest, L. (1997). The pharmacology of ryanodine and related compounds. *Pharmacol. Rev.* **49**, 53–98.
- Trepanier, C. H., Jackson, M. F. and MacDonald, J. F. (2012). Regulation of NMDA receptors by the tyrosine kinase Fyn. *FEBS J.* **279**, 12–19.
- Um, J. W., Nygaard, H. B., Heiss, J. K., Kostylev, M. A., Stagi, M., Vortmeyer, A., Wisniewski, T., Gunther, E. C. and Strittmatter, S. M. (2012). Alzheimer amyloid- $\beta$  oligomer bound to postsynaptic prion protein activates Fyn to impair neurons. *Nat. Neurosci.* **15**, 1227–1235.
- Um, J. W., Kaufman, A. C., Kostylev, M., Heiss, J. K., Stagi, M., Takahashi, H., Kerrisk, M. E., Vortmeyer, A., Wisniewski, T., Koleske, A. J. et al. (2013). Metabotropic glutamate receptor 5 is a coreceptor for Alzheimer  $\text{A}\beta$  oligomer bound to cellular prion protein. *Neuron* **79**, 887–902.
- Viles, J. H., Klewpatinond, M. and Nadal, R. C. (2008). Copper and the structural biology of the prion protein. *Biochem. Soc. Trans.* **36**, 1288–1292.
- Vyklický, L., Jr., Benveniste, M. and Mayer, M. L. (1990). Modulation of N-methyl-D-aspartic acid receptor desensitization by glycine in mouse cultured hippocampal neurones. *J. Physiol.* **428**, 313–331.
- Walz, R., Amaral, O. B., Rockenbach, I. C., Roesler, R., Izquierdo, I., Cavalheiro, E. A., Martins, V. R. and Brentani, R. R. (1999). Increased sensitivity to seizures in mice lacking cellular prion protein. *Epilepsia* **40**, 1679–1682.
- Watt, N. T., Taylor, D. R., Kerrigan, T. L., Griffiths, H. H., Rushworth, J. V., Whitehouse, I. J. and Hooper, N. M. (2012). Prion protein facilitates uptake of zinc into neuronal cells. *Nat. Commun.* **3**, 1134.
- Welinder, C. and Ekblad, L. (2011). Coomassie staining as loading control in Western blot analysis. *J. Proteome Res.* **10**, 1416–1419.
- Westergaard, L., Christensen, H. M. and Harris, D. A. (2007). The cellular prion protein (PrP<sup>C</sup>): its physiological function and role in disease. *Biochim. Biophys. Acta* **1772**, 629–644.
- You, H., Tsutsui, S., Hameed, S., Kannanayakal, T. J., Chen, L., Xia, P., Engbers, J. D. T., Lipton, S. A., Stys, P. K. and Zamponi, G. W. (2012).  $\text{A}\beta$  neurotoxicity depends on interactions between copper ions, prion protein, and N-methyl-D-aspartate receptors. *Proc. Natl. Acad. Sci. USA* **109**, 1737–1742.



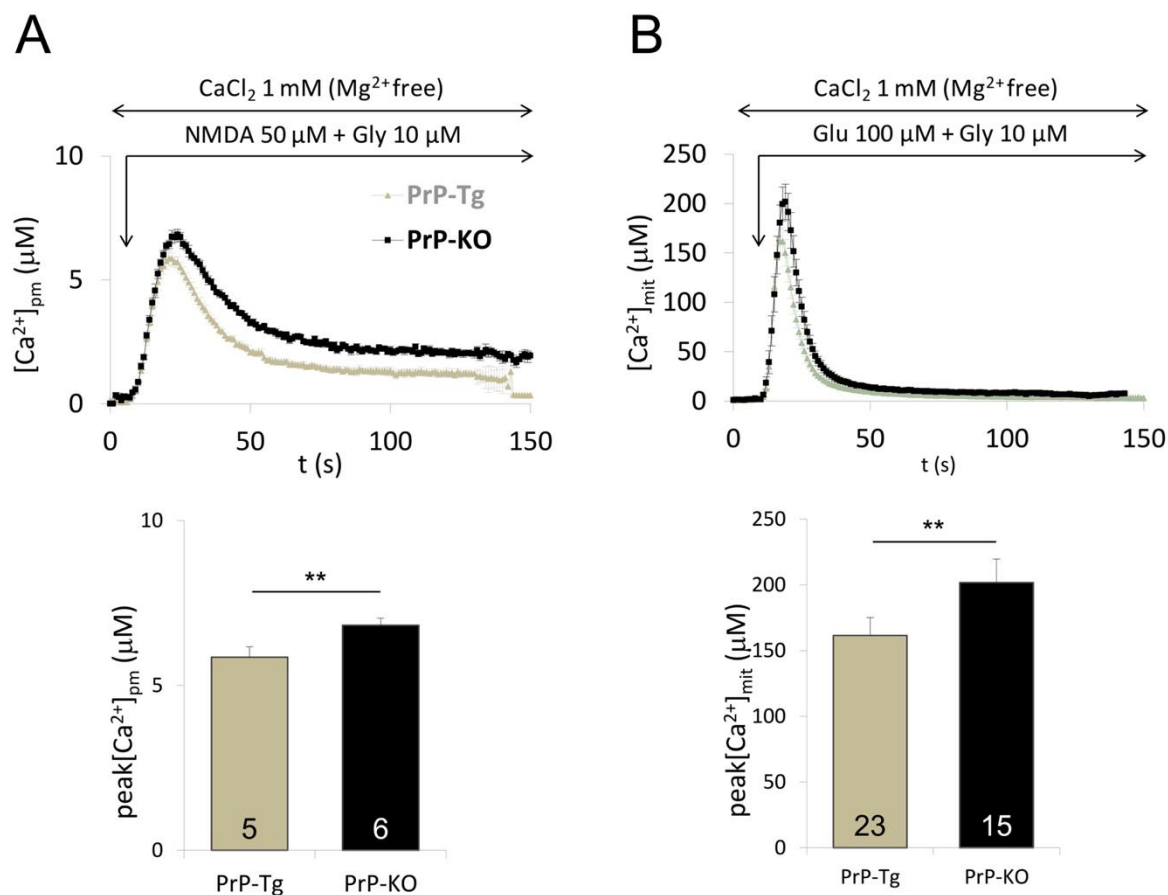


**Figure S1. PrP<sup>C</sup> attenuates Ca<sup>2+</sup> entry after NMDAR activation and glutamate-induced mitochondrial Ca<sup>2+</sup> transients in primary cortical neurons.** The kinetics of Ca<sup>2+</sup> transients (upper panels) and the peak value of Ca<sup>2+</sup> responses (lower panels) demonstrate that in cortical neurons PrP<sup>C</sup> (grey) reduced Ca<sup>2+</sup> accumulation in PM-subdomains after addition of NMDA (A), and mitochondrial Ca<sup>2+</sup> transients after addition of glutamate (Glu) (B) (both in the absence of Mg<sup>2+</sup> and in the presence of NMDAR co-agonist glycine (Gly), as indicated), compared to the PrP-KO counterpart (black). Here and after, values are expressed as mean  $\pm$  SEM, while the number of replicates is indicated inside each diagram bar. \*\* $p < 0.01$ ; here and after, statistics were performed by the Student's t-test, considering statistically significant a p-value  $< 0.05$ . Other details are as in the legend to Figs 1, 3 and 5.

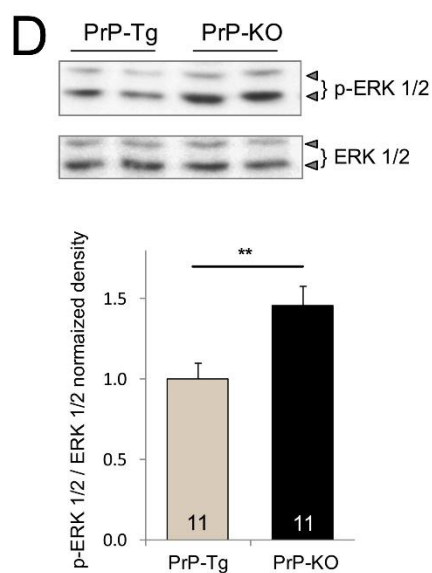
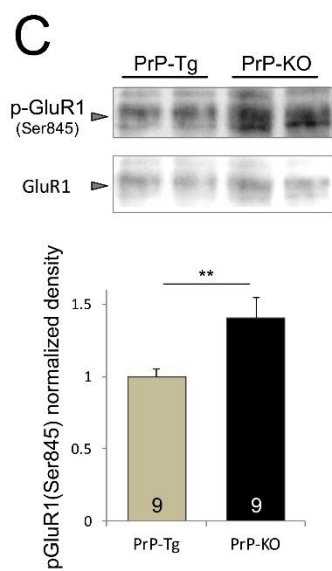
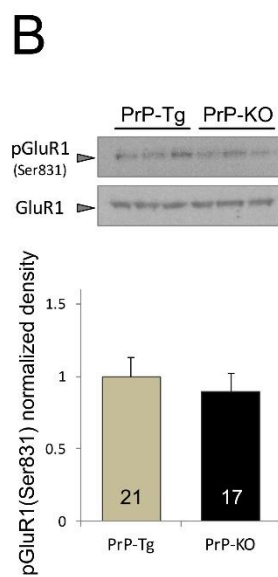
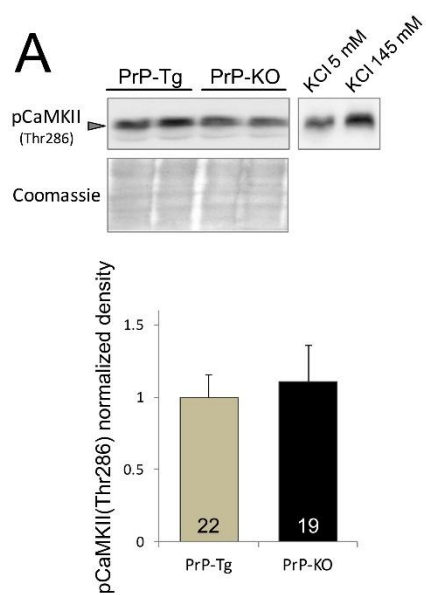


**Figure S2. PrP<sup>C</sup> does not affect the basal phosphorylation state of CaMKII on Thr286 nor the phosphorylation of AMPAR-GluR1 subunit on Ser831, while it downregulates phosphorylation of GluR1 on Ser845, and of ERK 1/2 on Thr202/Tyr204.** (A-D) Proteins (20 µg) from PrP-Tg and PrP-KO CGN lysates were resolved by SDS-PAGE, electroblotted and probed with antibody (Ab) to phosphorylated (p) CaMKII (on Thr286) (A), or to pGluR1(on Ser831) and GluR1 (B), or to pGluR1(on Ser845) and GluR1 (C), or to pERK 1/2 (on Thr202/Tyr204) and ERK 1/2 (D). Upper panels show Western blots (WB) for each genotype representative of at least 9 independent experiments (i.e., using cultures prepared in different days), while bar diagrams of the lower panels report the corresponding densitometric analyses. The optical density of pCaMKII immunoreactive bands was normalised to that of the corresponding Coomassie-stained lanes (A), while reliability of the anti-pCaMKII Ab was proved by the immunoreactive signal increase observed under depolarized conditions (KCl concentration raised to 145 mM) (upper-right panel), to allow Ca<sup>2+</sup> entry and CaMKII maximal stimulation. After normalisation of all immunosignals to the corresponding Coomassie-stained lanes (see Materials and Methods), the optical density of pGluR1Ser831 (B), pGluR1Ser845 (C), and pERK 1/2 (D), bands was normalised to that of the corresponding total GluR1 and ERK 1/2 bands, respectively. Incapacity of PrP<sup>C</sup> to regulate basal CaMKII activation (A) and (CaMKII-dependent) phosphorylation of AMPAR-GluR1Ser831 (B) strongly suggests that the different Ca<sup>2+</sup> fluxes observed in the two PrP genotypes upon stimulation with NMDA (Fig.1A) or AMPA (Fig.1C) cannot be explained by a CaMKII-dependent change in NMDAR recycling and AMPAR biophysical properties, respectively. Conversely, by downregulating PDE-inhibiting active ERK 1/2 levels (D), PrP<sup>C</sup> diminishes the (PKA-dependent) phosphorylation of AMPAR-GluR1Ser845 (C), which in turn lowers the presence of (GluR1-containing) receptors at the cell surface (see Fig. 3). All reported data were normalized to the values obtained with PrP-Tg samples. \*\*p < 0.01; other details are as in the legend to Fig. S1.



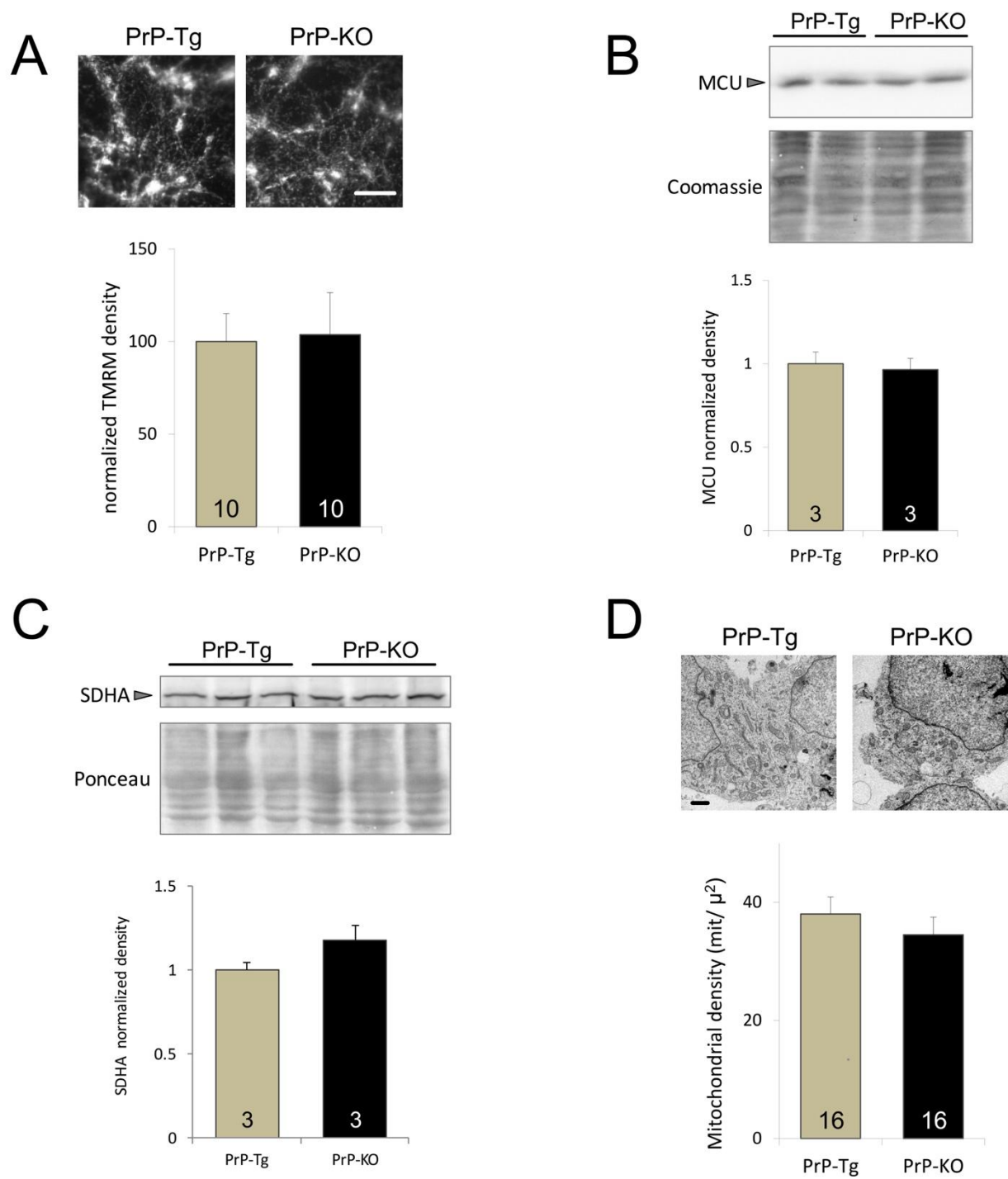


**Figure S3. The absence of PrP<sup>C</sup> does not modify Ca<sup>2+</sup>-related mitochondrial parameters, nor the number of the organelles.** (A, B) The amplitude of the mitochondrial membrane potential ( $\Delta\psi_m$ ) (A) and the expression of the Ca<sup>2+</sup> uniport (MCU) (B) were determined using the potentiometric fluorophore TMRM and WB, respectively. (A) Upper panels report representative fluorescence micrographs of TMRM-loaded CGN under basal conditions. The lower bar diagram reports the relative TMRM fluorescence quantification (expressed as percentage of the mean value obtained for PrP-Tg samples), indicating that both neuronal types had similar  $\Delta\psi_m$  magnitude. (B) The representative WB of PrP-Tg and PrP-KO CGN lysates (upper panels), probed with an Ab to MCU (i.e., to its channel-forming subunit), and the densitometric analyses (lower panel) – in which the MCU immunosignal was normalized to the optical density of the corresponding Coomassie-stained lanes and reported as fraction of the PrP-Tg mean value – clearly indicate that similar MCU amounts were present in both neuronal types. (C, D) Also the number of mitochondria was found to be similar in PrP-Tg and PrP-KO CGN. Indeed, no significant difference between the two genotypes was observed in: (i), the expression of the mitochondrial marker (inner membrane protein) succinate dehydrogenase-A (SDHA) (C), as shown by the representative WB (upper panels) and the corresponding densitometric analysis (lower panel), in which the SDHA immunosignal was normalized to the optical density of the corresponding Ponceau red-stained lanes; (ii), the mitochondrial density, assessed by transmission electron microscopy (TEM) analysis (D), as shown by the representative TEM micrographs (upper panels) and the quantification of the number of mitochondria per unit area (lower panel). Scale bar, 10  $\mu$ m in A; 1  $\mu$ m in D. Other details are as in the legend to Figs. S1 and S2.

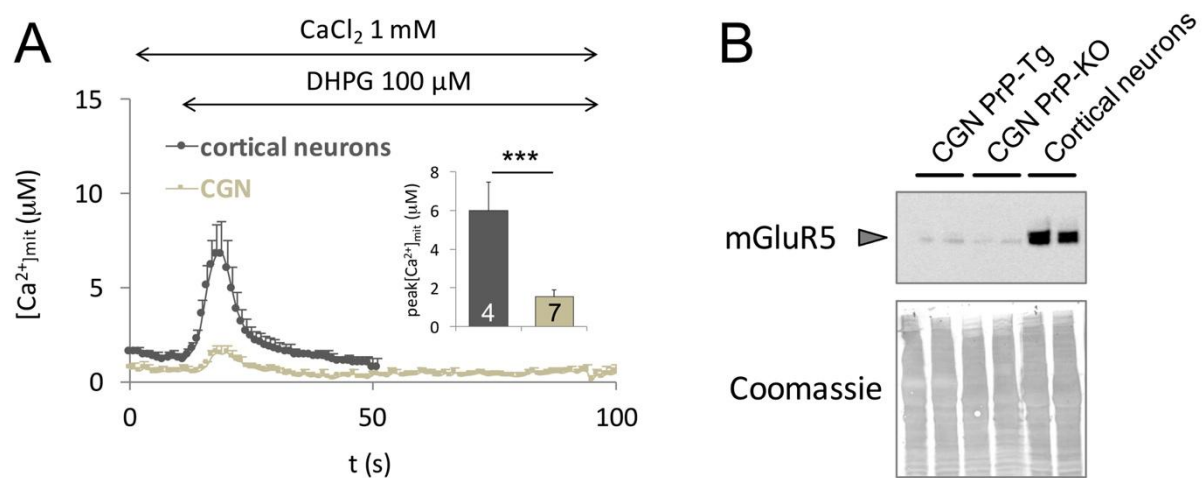


**Figure S4. mGluRs do not substantially contribute to glutamate-mediated mitochondrial Ca<sup>2+</sup> transients in CGN.** (A) DHPG, the specific agonist to mGluR1 and mGluR5, induced only minimal mitochondrial Ca<sup>2+</sup> transients in CGN and a much higher Ca<sup>2+</sup> transients in cortical neurons, as indicated by the average traces and the corresponding mean Ca<sup>2+</sup> peaks (bar diagrams, insets). (B) WB analysis of PrP-Tg and PrP-KO CGN and PrP-Tg cortical neurons (all run in duplicate) indicated that mGluR5 was robustly expressed in cortical neurons, but only slightly present in CGN (upper panel). All lysates were loaded in similar amounts, as shown by the corresponding lanes stained with Coomassie blue (lower panel). \*\*\**p* < 0.001; other details are as in the legend to Figs. S1 and S2.